

JYX



This is a self-archived version of an original article. This version may differ from the original in pagination and typographic details.

Author(s): ALICE Collaboration

Title: $K(892)0$ and $\phi(1020)$ production in p-Pb collisions at $\sqrt{s_{NN}} = 8.16$ TeV

Year: 2023

Version: Published version

Copyright: ©2023 CERN, for the ALICE Collaboration

Rights: CC BY 4.0


Rights url: <https://creativecommons.org/licenses/by/4.0/>

Please cite the original version:

ALICE Collaboration. (2023). $K(892)0$ and $\phi(1020)$ production in p-Pb collisions at $\sqrt{s_{NN}} = 8.16$ TeV. Physical Review C, 107(5), Article 055201. <https://doi.org/10.1103/PhysRevC.107.055201>

$K^*(892)^0$ and $\phi(1020)$ production in p -Pb collisions at $\sqrt{s_{NN}} = 8.16$ TeV

S. Acharya *et al.**
(ALICE Collaboration)

 (Received 28 October 2021; accepted 16 December 2022; published 9 May 2023)

The production of $K^*(892)^0$ and $\phi(1020)$ resonances has been measured in p -Pb collisions at $\sqrt{s_{NN}} = 8.16$ TeV using the ALICE detector. Resonances are reconstructed via their hadronic decay channels in the rapidity interval $-0.5 < y < 0$ and the transverse momentum spectra are measured for various multiplicity classes up to $p_T = 20$ GeV/c for $K^*(892)^0$ and $p_T = 16$ GeV/c for $\phi(1020)$. The p_T -integrated yields and mean transverse momenta are reported and compared with previous results in pp, p -Pb and Pb-Pb collisions. The x_T scaling for $K^*(892)^0$ and $\phi(1020)$ resonance production is newly tested in p -Pb collisions and found to hold in the high- p_T region at Large Hadron Collider energies. The nuclear modification factors (R_{pPb}) as a function of p_T for K^{*0} and ϕ at $\sqrt{s_{NN}} = 8.16$ TeV are presented along with the new R_{pPb} measurements of K^{*0} , ϕ , Ξ , and Ω at $\sqrt{s_{NN}} = 5.02$ TeV. At intermediate p_T (2–8 GeV/c), R_{pPb} of Ξ , Ω show a Cronin-like enhancement, while K^{*0} and ϕ show no or little nuclear modification. At high p_T (>8 GeV/c), the R_{pPb} values of all hadrons are consistent with unity within uncertainties. The R_{pPb} of $K^*(892)^0$ and $\phi(1020)$ at $\sqrt{s_{NN}} = 8.16$ and 5.02 TeV show no significant energy dependence.

DOI: [10.1103/PhysRevC.107.055201](https://doi.org/10.1103/PhysRevC.107.055201)

I. INTRODUCTION

High-energy heavy-ion (A-A) collisions provide a unique opportunity to study the deconfined quark-gluon plasma (QGP) created in such collisions [1–3]. The hot and dense medium created in heavy-ion collisions evolves with time and cools down to form a phase where hadron resonance gas is studied. Evidence at Relativistic Heavy Ion Collider (RHIC) and the Large Hadron Collider (LHC) suggest that the QGP phase is followed by a hadronic phase where the hadrons interact via rescattering and regeneration processes, before the final freeze-out. Resonances are short-lived hadrons that decay via the strong interactions. They play an important role to understand the particle production mechanisms and for the characterization of the dynamic evolution of the system formed in heavy-ion collisions. They are used as a sensitive probe of the hadronic phase, where their mass, width and yield could be modified due to interaction of their decay products through re-scattering and regeneration processes [4–15]. ALICE has previously measured $K^*(892)^0$ and $\phi(1020)$ production in pp collisions at $\sqrt{s} = 5.02, 7, 8,$ and 13 TeV [16–22], in p -Pb collisions at $\sqrt{s_{NN}} = 5.02$ TeV [23] and Pb-Pb collisions at $\sqrt{s_{NN}} = 2.76$ and 5.02 TeV [13,15,18,19].

Proton-lead collisions are intermediate between pp and Pb-Pb collisions in terms of the size of the colliding system

and the produced particle multiplicities. Recent measurements in high-multiplicity pp , p -Pb, and d -Au collisions at different energies have uncovered strong flowlike effects even in these small collision systems [14,22–25], whose origin is not fully understood. To investigate the mechanism of particle production and the origin of these effects, the ALICE Collaboration has studied the multiplicity dependence of light-flavor particle production for many species like π^\pm , K^\pm , K_s^0 , $K^*(892)^0$, $\phi(1020)$, Λ , $\Lambda(1520)$, $\Sigma^{*\pm}$, Ξ^\pm , Ξ^{*0} , Ω^\pm in p -Pb collisions at $\sqrt{s_{NN}} = 5.02$ TeV [23,26–29] and in pp collisions at $\sqrt{s} = 7$ and 13 TeV [17,20,22,30]. This paper reports on the multiplicity dependence of $K^*(892)^0$ and $\phi(1020)$ meson production at the highest center-of-mass energy, $\sqrt{s_{NN}} = 8.16$ TeV, reached at the LHC in p -Pb collisions. This provides an opportunity to extend the previous studies of production of these particles in p -Pb collisions at $\sqrt{s_{NN}} = 5.02$ TeV [23] to a higher multiplicity reach and a larger p_T coverage. Hadron production is governed by the soft and hard scattering processes at LHC energies. The bulk of particles produced in high-energy collisions is dominated by low transverse momentum particles from soft interactions, which are nonperturbative in nature. The yield of particles at low p_T is not well understood from the first principles of QCD and their description relies on phenomenological QCD-based models such as EPOS-LHC, DPMJET, and HIJING. The measurements in the low-momentum region of the spectra presented in this article provide input for the tuning of these event generators. In this paper, measurements of $K^*(892)^0$ and $\phi(1020)$ are compared with predictions from EPOS-LHC [31], DPMJET [32], and HIJING [33].

The transverse momentum spectra of light-flavor hadrons have shown a clear evolution with multiplicity in high-energy pp and p -Pb collisions [17,22,23,26,34], similar to that observed in Pb-Pb collisions [13,18,19,35,36], where in the latter

*Full author list given at the end of the article.

Published by the American Physical Society under the terms of the [Creative Commons Attribution 4.0 International](https://creativecommons.org/licenses/by/4.0/) license. Further distribution of this work must maintain attribution to the author(s) and the published article's title, journal citation, and DOI.

case the effect is usually attributed to a collective expansion of the system. The increase in slope of the p_T spectra as a function of multiplicity attributed to the radial flow is related to the low- p_T region of the spectrum, where flow is relevant. This feature is also reflected in an increase of the average transverse momentum $\langle p_T \rangle$ with multiplicity. In contrast to the yields dN/dy , which evolve smoothly as a function of multiplicity for different collision systems, the $\langle p_T \rangle$ of light-flavor hadrons as well as $K^*(892)^0$ and $\phi(1020)$, rises faster as a function of multiplicity in pp and p -Pb collisions than in Pb-Pb collisions, as discussed in Refs. [20,22,23]. The new measurements, with the highest multiplicity reach in p -Pb collisions, and comparison with the different model predictions can be used to further extend these studies.

The high- p_T particle production is analyzed within the framework of perturbative Quantum Chromodynamics (pQCD) which features a nearly scale-invariant behavior of elementary parton-parton hard-scattering processes [37,38]. The convolution of hard scattering cross-sections with the parton distribution functions (PDFs) of incident hadrons and fragmentation functions (FFs) leads to the observed scaling of the inclusive invariant cross-section $Ed^3\sigma/dp^3$ as p_T^{-n} at fixed transverse x , $x_T = 2p_T/\sqrt{s}$ [39,40]. The exponent n can be related to the scattering processes in which high- p_T hadrons are produced. If hadrons are produced by leading twist (LT) $2 \rightarrow 2$ hard subprocesses, then $n \approx 4$, and for higher twist (HT) processes, $n \approx 8$. It has been observed that the exponent value decreases with increasing collision energy, which suggests that the contribution of higher twist processes on high- p_T hadron production is reduced as a function of energy. The transverse momentum distributions of different particle species at high p_T are observed to satisfy a universal x_T scaling over a wide energy range up to $\sqrt{s} = 13$ TeV. This scaling behavior was observed by the CDF [41–43] and UA1 [44] Collaborations in $p(\bar{p})$ collisions, and by the STAR [45], ALICE [46], and CMS [47] Collaborations in pp collisions. In this paper, the x_T scaling of $K^*(892)^0$ and $\phi(1020)$ mesons are tested in p -Pb collisions at LHC energies. The transverse momentum distributions of the particles in p -Pb collisions are compared to those in pp collisions using the nuclear modification factor (R_{pPb}). The measurement of R_{pPb} acts as a control experiment observable in p -Pb collisions [48] in the context of the observed high- p_T hadron suppression in Pb-Pb collisions [15]. In this paper, R_{pPb} measurements of $K^*(892)^0$ and $\phi(1020)$ in p -Pb collisions at $\sqrt{s_{NN}} = 5.02$ and 8.16 TeV, and that of Ξ and Ω in p -Pb collisions at 5.02 TeV are reported. Similar measurements are also reported for strange and multistrange hadrons by CMS [49], and for π^\pm , K^\pm , and $p(\bar{p})$ by ALICE [26] in p -Pb collisions at $\sqrt{s_{NN}} = 5.02$ TeV. At high p_T (> 8 GeV/c), the values of R_{pPb} for all light hadrons are similar and found to be consistent with unity within the uncertainties. At intermediate p_T ($2 < p_T < 8$ GeV/c), the values of R_{pPb} for strange baryons (Ξ , Ω) show an enhancement with a clear mass dependence [49]. In this p_T region, the hard scattering processes start to dominate over soft processes and the momentum range where this transition may happen depend on the mass and quark composition of the particle species. The measurements of strange particles produced in high multiplicity p -Pb collisions [27,50] sug-

gested the presence of radial flow [51]. Due to the radial flow effect, hadrons of greater mass are pushed towards the higher transverse momentum and the effect increases with hadron mass as well as multiplicity [23,51]. However, it should be noted that some final state effects such as color reconnection in PYTHIA [52] which can mimic the radial flowlike effect and EPOS-LHC [31] which uses parameterized flow could describe the modification of transverse momentum spectra. The difference in the production mechanism of baryon and meson has been observed in particle ratios [23,51] and the nuclear modification factors [25,26,45,49,53]. The enhanced production of baryon ($R_{pPb} > 1$) may happen as a result of hadronization by parton recombination [54]. In addition, there are several initial-state effects such as isospin effect, Cronin effect, cold-nuclear matter energy loss and nuclear shadowing that can result in $R_{pPb} \neq 1$ [55]. The Cronin enhancement [56] in the intermediate p_T are reported in the low-energy experiments [57,58]. Similar enhancement is observed for (anti)proton compared to pion and kaon in p -Pb collisions at $\sqrt{s_{NN}} = 5.02$ TeV [26]. In this paper, the particle species and collision energy dependence of R_{pPb} is studied for p -Pb collisions at LHC energies.

Throughout this paper, the results for $K^*(892)^0$ and $\bar{K}^*(892)^0$ are averaged and denoted by the symbol K^{*0} , while $\phi(1020)$ is denoted by ϕ . The paper is organized as follows. In Sec. II, the dataset, event, and track selection criteria; the analysis techniques; the procedure for extraction of the yields; and the study of the systematic uncertainties are briefly discussed. In Sec. III, the results on the transverse momentum spectra, the dN/dy , $\langle p_T \rangle$, x_T scaling, and R_{pPb} in p -Pb collisions at $\sqrt{s_{NN}} = 8.16$ TeV are presented. Finally, the results are summarized in Sec. IV.

II. DATA ANALYSIS

The measurements of K^{*0} and ϕ meson production in p -Pb collisions at $\sqrt{s_{NN}} = 8.16$ TeV have been performed on data collected with the ALICE detector in the year 2016. The resonances are reconstructed via their hadronic decay channels with branching ratios (BR) of 66.6% for $K^{*0} \rightarrow \pi^\pm K^\mp$ and 49.2% for $\phi \rightarrow K^+ K^-$ in the rapidity interval $-0.5 < y < 0$, where y stands for the rapidity in the nucleon-nucleon center-of-mass. For both K^{*0} and ϕ , the analysis is performed in various multiplicity classes and also using a multiplicity-integrated sample.

A. Event selection

The detailed description of the ALICE detector setup and its performance can be found in Refs. [59,60]. In p -Pb configurations, the ^{208}Pb beam circulates towards the positive z direction in the ALICE laboratory frame, while the proton beam circulates in the opposite direction. Due to the asymmetric system, the center-of-mass frame is shifted in the rapidity by $\Delta y = -0.465$ in the direction of the proton beam with respect to the laboratory frame. The minimum bias trigger was configured to select events by requiring at least a coincidence signal in both the V0A and V0C detectors [61,62]. The V0 detector system consists of two arrays of 32 scintillator

TABLE I. Mean charged particle multiplicity densities ($\langle dN_{\text{ch}}/d\eta \rangle$) measured in pseudorapidity range $|\eta_{\text{lab}}| < 0.5$, corresponding to the various multiplicity classes defined using the V0A detector in p -Pb collisions at $\sqrt{s_{\text{NN}}} = 8.16$ TeV [62].

V0A percentile (%)	$\langle dN_{\text{ch}}/d\eta \rangle_{ \eta_{\text{lab}} < 0.5}$
0–5	53.22 ± 1.38
5–10	42.40 ± 1.10
10–20	35.49 ± 0.92
20–40	26.89 ± 0.70
40–60	18.39 ± 0.48
60–80	10.97 ± 0.29
80–100	4.47 ± 0.14

detectors, one on each side of the interaction point covering the full azimuthal angle in the pseudorapidity regions $2.8 < \eta < 5.1$ (V0A) and $-3.7 < \eta < -1.7$ (V0C). The background events due to beam-gas interaction and other machine-induced background collisions are rejected using the timing information from the V0 and the zero degree calorimeter (ZDC) [60]. The primary vertex of a collision is determined using charged tracks reconstructed in the inner tracking system (ITS) [63] and the time projection chamber (TPC) [64]. The events are selected whose primary vertex position along the beam axis (v_z , z is the longitudinal direction) is within ± 10 cm from the nominal interaction point. Pileup events from the triggered bunch crossing are rejected if multiple collision vertices are identified in the silicon pixel detector (SPD), which is the innermost detector of the ITS [60,64]. The total number of events analyzed after applying the event selection criteria is about 30 million. The minimum bias events are further divided into seven multiplicity classes, according to the total charge deposited in the forward V0A detector [61]. The yield of K^{*0} and ϕ are measured in the rapidity interval $-0.5 < y < 0$ for the following event multiplicity classes, 0–5%, 5–10%, 10–20%, 20–40%, 40–60%, 60–80%, and 80–100%. The p_T spectra normalized to the fraction of non-single-diffractive (NSD) events are also obtained for both K^{*0} and ϕ . The mean charged-particle multiplicity ($\langle dN_{\text{ch}}/d\eta \rangle$) corresponding to each multiplicity class, and measured in the pseudorapidity interval $|\eta_{\text{lab}}| < 0.5$, is given in Table I taken from Ref. [62].

B. Track selection and particle identification

The charged tracks coming from the primary vertex are selected in the pseudorapidity interval $|\eta| < 0.8$ with $p_T > 0.15$ GeV/c. This ensures the uniform acceptance for the central barrel detectors. The high quality tracks are chosen based on selection criteria as done previously in Ref. [23]. The K^{*0} and ϕ mesons are reconstructed from the charged tracks which have crossed at least 70 of a maximum 159 horizontal segments along the transverse readout plane of the TPC. The contamination from secondary particles originating from weak decays and beam background events are reduced by applying a selection on the distance of closest approach to the primary vertex in the transverse plane (DCA_{xy}) and

along the longitudinal direction (DCA_z). A p_T -dependent cut of $\text{DCA}_{xy}(p_T) < (0.0105 + 0.035p_T^{-1.1})$ cm, with p_T in GeV/c, is used, which is less than 7 times its resolution. The track DCA_z is required to be less than 2 cm [65]. The decay daughters (pions and kaons) of resonances are identified by measuring the specific ionization energy loss (dE/dx) in the detector gas of the TPC and their time-of-flight information using the TOF [66]. The dE/dx resolution of the TPC is denoted as σ_{TPC} and the charged tracks are identified as pions and kaons if the mean specific energy loss measured by the TPC is within $6\sigma_{\text{TPC}}$, $3\sigma_{\text{TPC}}$, and $2\sigma_{\text{TPC}}$ from the expected $\langle dE/dx \rangle$ values in the momentum range $p < 0.3$ GeV/c, $0.3 < p < 0.5$ GeV/c, and $p > 0.5$ GeV/c, respectively. In addition to the TPC, if the TOF information is available, then the charged tracks are identified by requiring the time-of-flight values within $3\sigma_{\text{TOF}}$ of the expected values for the full momentum range.

C. Yield extraction

The K^{*0} and ϕ resonances are reconstructed from their decay products using the invariant mass technique. The invariant mass distributions are obtained from unlike charge πK (for K^{*0}) and KK (for ϕ) pairs in the same event. The distributions exhibit a signal peak and a large combinatorial background from the uncorrelated πK (KK) pairs. The combinatorial background is estimated using two methods, mixed-event and like-sign. In the mixed-event method, the tracks from one event are paired with oppositely charged tracks from other events. Each event is mixed with five other events to reduce the contribution of statistical uncertainty from the background distribution. The events which are mixed are selected to have similar characteristics like the longitudinal position of primary vertex (v_z) must differ by less than 1 cm and the multiplicity percentiles computed using the V0A amplitude must differ by less than 5%. The mixed-event distributions for K^{*0} (ϕ) are normalized in the mass region $1.1 < m_{\text{inv}} < 1.15$ GeV/ c^2 ($1.04 < m_{\text{inv}} < 1.15$ GeV/ c^2) that is approximately five σ away from the mass peak of each particle. In the like-sign method, tracks of identical charges from the same events are paired and the invariant mass distribution for the uncorrelated background is obtained as the geometric mean $2\sqrt{n^{++} \times n^{--}}$, where n^{++} and n^{--} are the number of positive-positive and negative-negative pairs in each invariant mass bin, respectively. The mixed-event technique is the default method used for the extraction of yield both for K^{*0} and ϕ , whereas the like-sign background is used for the estimation of the systematic uncertainty. Figures 1(a) and 1(b) show the invariant mass distributions of $\pi^{\mp}K^{\pm}$ and K^+K^- pairs from the same events and the mixed-events in the transverse momentum interval $1.4 \leq p_T < 1.6$ and $0.6 \leq p_T < 0.8$ GeV/c for 0–100% in p -Pb collisions, respectively. The $\pi^{\mp}K^{\pm}$ and K^+K^- invariant mass distributions after mixed-event background subtraction are shown in Figs. 1(c) and 1(d), respectively, where the characteristic signal peak is observed on top of the residual background. The residual background arises due to correlated pairs from jets, misidentification of the decay daughters of resonances and decay of other particles [23]. The raw yields of resonances are extracted in each p_T bin and multiplicity

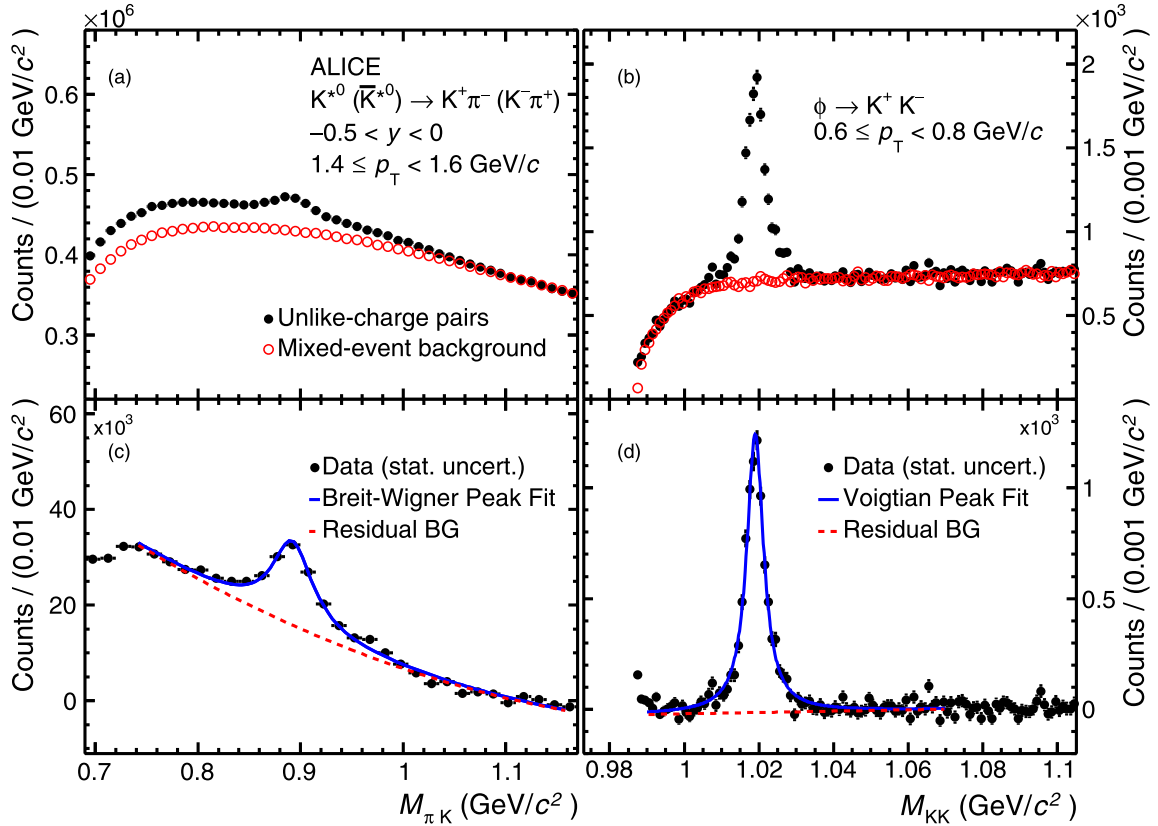


FIG. 1. Invariant mass distributions for K^{*0} and ϕ in the multiplicity class 0–100% and transverse momentum range $1.4 \leq p_T < 1.6$ GeV/c and $0.6 \leq p_T < 0.8$ GeV/c, respectively. In panels (a), (b), black markers show the unlike-sign invariant mass distributions and red markers show the normalized mixed event background. After the background subtraction the signals are shown in panels (c), (d). The K^{*0} peak is described by a Breit-Wigner function, whereas the ϕ peak is fitted with a Voigtian function. The residual background is described by the second-order polynomial function.

class. The signal peak is fitted with a Breit-Wigner and a Voigtian function (convolution of Breit-Wigner and Gaussian functions) for K^{*0} and ϕ , respectively. A second-order polynomial function is used to describe the shape of the residual background for both resonances. The signal peak fit is performed in the range $0.75 < M_{K\pi} < 1.15$ GeV/c² ($0.99 < M_{KK} < 1.07$ GeV/c²) for K^{*0} (ϕ). The widths of the K^{*0} and ϕ are fixed to their PDG values $\Gamma(K^{*0}) = 47.4 \pm 0.6$ MeV/c², $\Gamma(\phi) = 4.26 \pm 0.04$ MeV/c² [67], whereas the resolution parameter of the Voigtian function for ϕ is kept as a free parameter. The measured resolution of the ϕ mass as a function of p_T (σ of Gaussian) varies between 1 and 3 MeV/c². The sensitivity to the choice of the fitting range, the normalization interval, the shape of the background function, the width and resolution parameters have been studied by varying the default settings, as described in Sec. II D. In minimum bias collisions, K^{*0} (ϕ) production is measured in the p_T range from 0 to 20 GeV/c (0.4 to 16 GeV/c). With the available data samples, K^{*0} production is measured up to $p_T = 15$ GeV/c in 0–5% and 5–10%, up to $p_T = 20$ GeV/c in 10–20%, 20–40%, and 40–60%, up to 10 GeV/c in 60–80% and up to 6 GeV/c in 80–100% multiplicity classes, while the ϕ production is measured up to $p_T = 16$ GeV/c in 0–5%, 5–10%, 10–20%, 20–40%, $p_T = 12$ GeV/c in 40–60%, $p_T = 10$ GeV/c in 60–80%, and $p_T = 6$ GeV/c in 80–100% multiplicity class.

The raw transverse momentum distributions are normalized by the number of accepted events and corrected for the branching ratio, detector acceptance and reconstruction efficiency ($A \times \epsilon_{\text{rec}}$) and, signal loss. The correction factor due to the vertex reconstruction efficiency is negligible in all multiplicity classes. The $A \times \epsilon_{\text{rec}}$ is obtained from the Monte Carlo simulation (MC) based on the DPMJET [32] event generator and the interaction of the generated particles passing through the ALICE detector geometry is modeled using GEANT3 [68]. It is defined as the ratio of the reconstructed K^{*0} (ϕ) to the generated K^{*0} (ϕ), both in the rapidity interval $-0.5 < y < 0$, and determined as a function of p_T . The same track and particle identification (PID) selection criteria are applied to the decay daughter of resonances in MC as are used in the analysis. The shape of the generated p_T distributions are different from the measured p_T distributions, therefore a re-weighting procedure is used, in which the generated distributions are weighted to match the measured distributions. The effect of the reweighting procedure on $A \times \epsilon_{\text{rec}}$ is ≈ 2 –5% at low p_T (< 1 GeV/c) and negligible for $p_T > 1$ GeV/c. The reweighted $A \times \epsilon_{\text{rec}}$ is used to correct the raw p_T distribution. No significant multiplicity dependence of $A \times \epsilon_{\text{rec}}$ is observed, therefore the raw p_T spectra in the various multiplicity classes are corrected with the minimum bias $A \times \epsilon_{\text{rec}}$ values. The signal loss corrections that account for the loss in K^{*0} and ϕ yields caused

TABLE II. The sources of systematic uncertainties for K^{*0} and ϕ yields in p -Pb collisions at $\sqrt{s_{NN}} = 8.16$ TeV. For each source, the average uncertainties are listed for the low and high- p_T intervals.

Systematic variation	K^{*0}		ϕ	
	p_T (GeV/c)			
	0.0–4.0	4.0–20.0	0.4–4.0	4.0–16.0
Yield extraction (%)	7.5	8.0	2.8	4.5
Track selection (%)	3.0	2.0	4.4	5.5
Particle identification (%)	4.3	5.0	1.9	3.5
Global tracking efficiency (%)	2.0	3.2	2.0	2.3
Material budget (%)	1.2	<0.5	2.2	<0.5
Hadronic Interaction (%)	1.9	<0.5	2.4	<1
Total (%)	9.6	10.2	6.7	8.3

by the event selection with minimum bias trigger, rather than all NSD events, are found to be negligible in the measured p_T range. The minimum bias p_T spectra are normalized to the fraction of NSD events, which is 0.992.

D. Systematic uncertainties

The sources of systematic uncertainties of the measurement of K^{*0} and ϕ production are signal extraction, track selection criteria, particle identification, global tracking efficiency, uncertainty in the material budget of the ALICE detector and the hadronic interaction cross-section in the detector material. A similar approach is adopted as used for the systematic uncertainty study of K^{*0} and ϕ in p -Pb collisions at $\sqrt{s_{NN}} = 5.02$ TeV [23]. No multiplicity dependence of the systematic effects is observed, therefore the systematic uncertainties of minimum bias p_T spectra are propagated for all multiplicity event classes studied. A summary of systematic uncertainties for K^{*0} (ϕ) in two transverse momentum intervals, $0 < p_T < 4$ GeV/c ($0.4 < p_T < 4$ GeV/c) and $4 < p_T < 20$ GeV/c ($4 < p_T < 16$ GeV/c) are given in Table II. The uncertainties due to signal extraction include variations of the signal peak fitting range, variations of width and mass resolution, mixed-event background normalization region, choice of residual background function, and combinatorial background. The fitting range of the πK (KK) invariant mass distribution is varied by ≈ 50 (5) MeV/c² on each side of the signal peak. The normalization range of the πK (KK) invariant mass distributions differed by approximately 150 (50) MeV/c² with respect to the default value. The width of the resonances is fixed for the default fit whereas it is kept free for systematic studies. The residual background is fitted with a first-order and third-order polynomial function for the systematic studies of the signal extraction. For ϕ resonance, the effect of the variation of the resolution parameter (σ of the Gaussian) on the yield is also included in the systematic uncertainties. The combinatorial background from the like-sign method is used for systematic studies. The contribution of systematic uncertainties due to the signal extraction is 7.5–8% for K^{*0} and 2.8–4.5% for ϕ . The systematic effects due to the charged track selection are studied by varying the criteria based on the number of crossed readout rows in the TPC and

the distance of closest approach to the primary vertex of the collision [65]. The relative contribution of uncertainties due to the track selection are 2–3% for K^{*0} and about 4.4–5.5% for the ϕ . For the PID systematic uncertainty, the selections based on the TPC dE/dx and TOF time-of-flight are varied. Three variations are taken where one is a momentum dependent PID selection of $5\sigma_{\text{TPC}}$ ($0 < p < 0.3$), $2.5\sigma_{\text{TPC}}$ ($0.3 < p < 0.5$), $1.5\sigma_{\text{TPC}}$ ($p > 0.5$) with $3\sigma_{\text{TOF}}$, and two momentum-independent selection; $2\sigma_{\text{TPC}}$ with $3\sigma_{\text{TOF}}$ and $2\sigma_{\text{TPC}}$ only, for both K^{*0} and ϕ . This results in systematic uncertainties of 4.3–5% for K^{*0} and 1.9–3.5% for the ϕ . The uncertainty related to global tracking arises from the difference in the ITS-TPC track matching efficiency in data and MC. It is estimated from the single charged track uncertainty by taking the linear sum of the uncertainties of the two charged tracks which are used to reconstruct the resonances. It contributes to the systematic uncertainties with 2–3.2% and 2–2.3% for K^{*0} and ϕ , respectively. The material budget systematic effects account for the uncertainties in the estimation of the ALICE detector material budget and is estimated to be 1.2% for K^{*0} and 2.2% for ϕ at low p_T . It is negligible at $p_T > 4$ GeV/c for both K^{*0} and ϕ . The systematic uncertainty due to the hadronic interaction cross-section in the detector material is estimated to be 1.9% for K^{*0} and 2.4% for ϕ at low p_T , and negligible for $p_T > 4$ GeV/c. The effects of material budget and hadronic interaction are evaluated by combining the uncertainties of the two charged tracks (π , K for K^{*0} and two K for ϕ) according to the kinematics of the decay. The systematic uncertainties of the material budget and the hadronic interaction cross-section were taken from Ref. [23]. The total systematic uncertainty is taken as the quadratic sum of all contributions and varies as 9.6–10.2% for K^{*0} and 6.7–8.3% for ϕ . The sources of systematic uncertainties that are multiplicity-dependent and uncorrelated across different multiplicity classes are also estimated. The systematic uncertainties due to signal extraction and PID are fully uncorrelated, whereas global tracking, track selection criteria, material budget and hadronic cross-section are correlated among event multiplicity classes.

III. RESULTS AND DISCUSSION

A. Transverse momentum spectra

The measurement of K^{*0} (ϕ) production performed in the rapidity interval $-0.5 < y < 0$ up to $p_T = 20$ (16) GeV/c in p -Pb collisions at $\sqrt{s_{NN}} = 8.16$ TeV is reported. Figure 2 shows p_T spectra of K^{*0} (left panel) and ϕ (right panel) for NSD events. These are compared with the predictions from EPOS-LHC [31,69], DPMJET [32], and HIJING [33] models. The bottom panels of Fig. 2 show the ratios of p_T spectra from these models to the data. The EPOS Monte Carlo event generator is a hadronic interaction parton model based on Gribov’s Reggeon field theory formalism which includes the feature of collective hadronization and the core-corona mechanism from pp to A-A collisions [70–72]. If the string segments of the final state parton have high-energy density, then that region is known as the “core,” whereas the region with strings of low-energy density surrounding the core

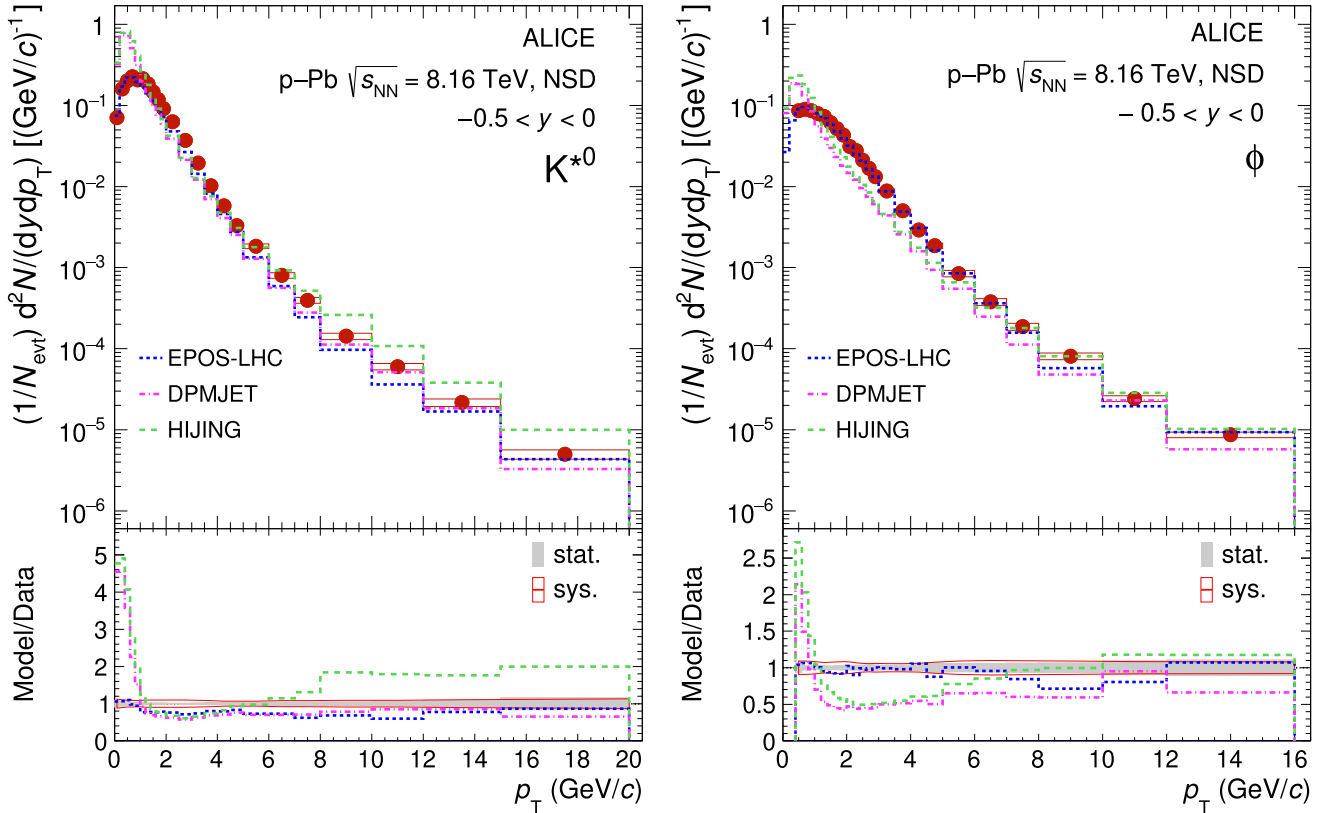


FIG. 2. Top panels: Transverse momentum spectrum of K^{*0} (left) and ϕ (right) as a function of p_T for the NSD events, measured in the rapidity interval $-0.5 < y < 0$ for p -Pb collisions at $\sqrt{s_{NN}} = 8.16$ TeV. The statistical and systematic uncertainties are shown as bars and boxes, respectively. The NSD spectrum is compared with the predictions from EPOS-LHC [31,69], DPMJET [32], and HIJING [33]. Bottom panels: The ratios of p_T spectra from model to data. The shaded bands around unity describe the statistical and systematic uncertainties of the data point.

is called the “corona.” The core evolves hydrodynamically and subsequently hadronizes to form the bulk of the system whereas the strings in the corona region break through the production of quark-antiquark pairs, which hadronize as fragmentation processes in vacuum. EPOS-LHC [31] is a tune of EPOS1.99 [73] that incorporates a parametrization of flow based on LHC data. The EPOS1.99 model is different from EPOS2.x [74] and EPOS3.x [69] as it does not use the complete 3D hydro calculation followed by the hadronic cascade but instead relies on the fast covariant approach. It describes various observables in minimum bias heavy-ion collisions as well as small collision systems up to a few GeV/c at LHC energies. DPMJET is a QCD-inspired dual parton model based on the Gribov-Glauber approach that treats the soft and hard scattering interaction processes differently. HIJING combines the perturbative QCD process with soft excitation, the production of multiple minijets, the interactions of jets in dense hadronic matter, and nuclear shadowing of parton distribution functions. For the K^{*0} resonance, at low p_T (< 1 GeV/c), DPMJET and HIJING models overestimate the data, whereas EPOS-LHC model gives a good description of the p_T spectrum. At $p_T > 1$ GeV/c, DPMJET and EPOS-LHC underestimate and closer to the data, however HIJING model underestimates (similar to the DPMJET and EPOS-LHC) for $1 < p_T < 5$ GeV/c and overestimates for $p_T > 5$ GeV/c.

The EPOS-LHC model describes the ϕ p_T spectrum relatively better than the DPMJET and HIJING for all p_T . However, HIJING model gives a good description of p_T distribution of ϕ resonance for $p_T > 6$ GeV/c. The EPOS-LHC model, where a different parametrization of flow is introduced in small collision systems like pp than the large volume produced in heavy-ion collisions, gives a better description of the transverse momentum distributions for both K^{*0} and ϕ in p -Pb collisions. Figure 3 shows the $\sqrt{s_{NN}}$ dependence of the transverse momentum spectra of K^{*0} and ϕ for NSD events in p -Pb collisions. The upper panels of Fig. 3 show a comparison of the transverse momentum spectra of K^{*0} and ϕ at $\sqrt{s_{NN}} = 5.02$ and 8.16 TeV, whereas the lower panels show the ratio of the p_T -differential yield at $\sqrt{s_{NN}} = 8.16$ to 5.02 TeV and its comparison with the results obtained from models [31–33,69]. The uncertainties of the ratios are obtained as the sum in quadrature of the uncertainties of the spectra at the two energies, which are largely uncorrelated. Up to p_T 1 GeV/c, the differential yield ratio seems to independent of p_T and collision energy. The values are consistent with unity within uncertainties. It suggests that the particle production in the soft scattering region is not strongly dependent on collision energy. The differential yield ratios increases as a function of p_T for $p_T \gtrsim 1$ GeV/c. Similar behavior is also observed in pp collisions in Ref. [21]. The p_T differential yield ratios

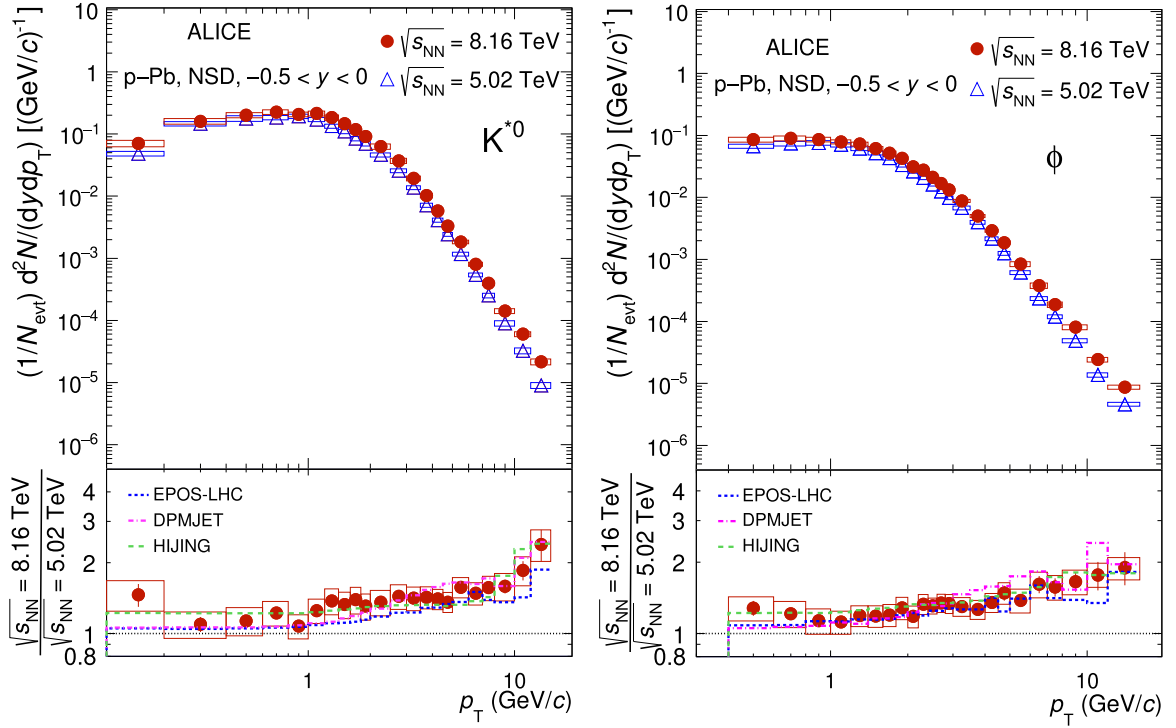


FIG. 3. Top panels: Energy dependence comparison of the transverse momentum spectra of K^{*0} (left) and ϕ (right) as a function of p_T for the NSD events, measured in the rapidity interval $-0.5 < y < 0$ for p -Pb collisions at $\sqrt{s_{NN}} = 5.02$ and 8.16 TeV. Bottom panels: The ratio of p_T spectrum at $\sqrt{s_{NN}} = 8.16$ TeV to the p_T spectrum at $\sqrt{s_{NN}} = 5.02$ TeV. The ratio is compared with the predictions from EPOS-LHC [31,69], DPMJET [32], and HIJING [33]. The statistical and systematic uncertainties are shown as bars and boxes, respectively.

obtained from EPOS-LHC, DPMJET, and HIJING are consistent with the measurements within the systematic uncertainties and reproduce well the energy dependence trend for K^{*0} and ϕ in p -Pb collisions. Figure 4 shows the transverse momentum distributions of K^{*0} (left panel) and ϕ (right panel) in various multiplicity classes. The ratios of p_T spectra in various multiplicity classes to the p_T spectrum for NSD events are shown in the bottom panels of Fig. 4. For $p_T \lesssim 4$ GeV/c, the slopes of the p_T spectra increase from low to high multiplicity classes, whereas the spectral shapes are similar at high p_T for all multiplicity classes. This indicates that processes like radial flow, which lead to a change in the shape of the p_T spectra for various multiplicity classes, dominate mainly at low p_T [36]. The increase in the slope of p_T spectrum with multiplicity is reflected in Fig. 5 for $\langle p_T \rangle$ as a function of multiplicity. A similar behavior was also observed for K^{*0} and ϕ in p -Pb collisions [23] at $\sqrt{s_{NN}} = 5.02$ TeV. The hardening of the p_T spectra with charged particle multiplicity was also reported for inclusive charged hadron spectra, π , K , p , K_S^0 , Λ , Ξ , and Ω in pp collisions at LHC energies [20,22,34,75], where different models with multiparton interactions were shown to describe these effects.

B. Integrated particle yield and mean transverse momentum

The p_T -integrated yields and mean transverse momentum are extracted from transverse momentum spectra in the measured range and using the fit function in the unmeasured region. The ϕ yield is extrapolated in the unmeasured re-

gion ($p_T < 0.4$ GeV/c) by fitting a Lévy-Tsallis functions [76] to the measured p_T spectra in all multiplicity classes. The difference in the yield contribution at low p_T due to different fitting functions (i.e., exponential, Boltzmann, m_T -exponential, Bose-Einstein and Boltzmann-Gibbs Blast-Wave function in Ref. [46]) from the Lévy-Tsallis function is included in the systematic uncertainties. The low- p_T extrapolation accounts for 8.9% (14.1%) of the total yield in the 0–5% (80–100%) multiplicity class. The K^{*0} spectra are measured from $p_T = 0$, so low- p_T extrapolation is not needed. The contribution of the extrapolated fraction of the yield is negligible for $p_T > 20$ GeV/c (16 GeV/c) for K^{*0} (ϕ). The values of dN/dy and $\langle p_T \rangle$ of K^{*0} and ϕ for various multiplicity classes are summarized in the Table III. The multiplicity-scaled integrated yields $[(dN/dy)/(\langle dN_{ch}/d\eta \rangle_{|\eta|<0.5})]$ for K^{*0} and ϕ are shown in the upper panels of Fig. 5 as a function of $\langle dN_{ch}/d\eta \rangle_{|\eta|<0.5}$. These results are compared with other ALICE measurements in pp collisions at $\sqrt{s} = 7$ and 13 TeV [20,22], in p -Pb collisions at $\sqrt{s_{NN}} = 5.02$ TeV [23], and in Pb-Pb collisions at $\sqrt{s_{NN}} = 2.76$ and 5.02 TeV [15,18,19]. The scaled integrated yields evolve smoothly as a function of multiplicity from pp , p -Pb to Pb-Pb collisions. For similar $\langle dN_{ch}/d\eta \rangle_{|\eta|<0.5}$, these values are consistent within uncertainties for different colliding systems and at various LHC energies. This indicates that event multiplicity drives the resonance production, irrespective of the colliding systems and energies [20,22,23].

The scaled integrated yields of ϕ show a slight increase with multiplicity from pp collisions to mid-central Pb-Pb

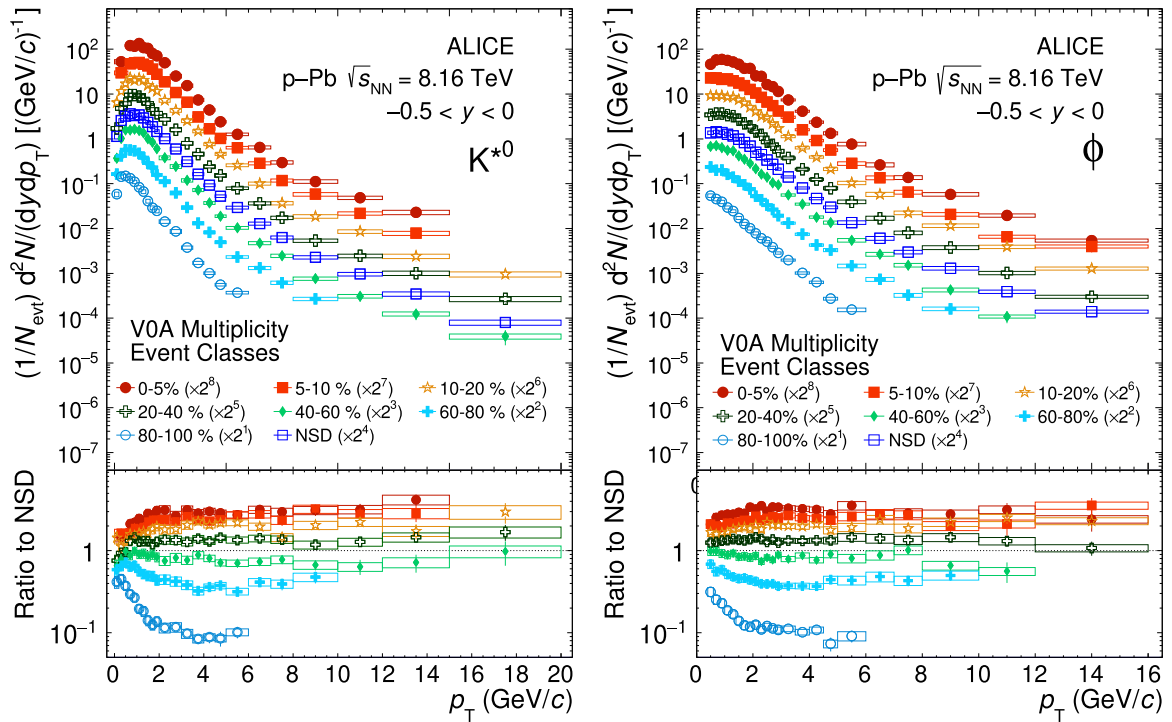


FIG. 4. Top panels: The transverse momentum spectra of K^{*0} (left) and ϕ (right) for various multiplicity classes, measured in the rapidity interval $-0.5 < y < 0$ for p -Pb collisions at $\sqrt{s_{NN}} = 8.16$ TeV. Bottom panels: The ratios of p_T spectra of given event multiplicity classes to the NSD spectra are shown. The statistical and systematic uncertainties are shown as bars and boxes, respectively.

collisions. The total increase is 12% with a 1.5σ significance between the lowest multiplicity bin and the highest multiplicity bin in p -Pb collisions at $\sqrt{s_{NN}} = 8.16$ TeV. Similarly scaled integrated yields of K^{*0} show a slight decrease with multiplicity for all three collision systems and the total decrease is 12% with a 1.8σ significance for p -Pb collisions at $\sqrt{s_{NN}} = 8.16$ TeV. The significance is calculated using statistical and multiplicity uncorrelated systematic uncertainties, added in quadrature. The integrated yield ratios of resonances relative to those of longer lived particles, π , K , and p are computed to study their production mechanism. The K^{*0}/K (ϕ/π) ratio measured in p -Pb collisions at $\sqrt{s_{NN}} = 5.02$ TeV [23] shows a decreasing (increasing) trend going from the lowest multiplicity to the highest multiplicity bin with a significance of 2.6σ (1.5σ) which is discussed in the context of a hint of a re-scattering (strangeness enhancement) effect. Future measurements of π and K yields in p -Pb collisions at $\sqrt{s_{NN}} = 8.16$ TeV will be useful to study these effects at higher center-of-mass energy and up to larger multiplicity. The model comparison with the p -Pb data shows that EPOS-LHC describes the scaled integrated yields for both K^{*0} and ϕ whereas HIJING overestimates the data for all multiplicities. The DPMJET model describes the scaled integrated yield of ϕ at higher multiplicities but overestimates the K^{*0} at all multiplicities. The $\langle p_T \rangle$ exhibits an increasing trend as a function of $\langle dN_{ch}/d\eta \rangle_{|\eta| < 0.5}$ for K^{*0} and ϕ in various colliding systems and energies as shown in the bottom panels of Fig 5. The increase in $\langle p_T \rangle$ is faster for pp and p -Pb than Pb-Pb and for a common multiplicity coverage the values

of $\langle p_T \rangle$ in pp and p -Pb are larger than Pb-Pb. At similar multiplicity ($\langle dN_{ch}/d\eta \rangle_{|\eta| < 0.5} \approx 40$), the difference in $\langle p_T \rangle$ values among Pb-Pb, p -Pb and pp collisions indicate that the geometry and dynamics of the collision systems are different, while the scaled integrated yields of K^{*0} and ϕ are similar for all colliding systems and energies. This indicates that the high multiplicity event sample in small collision systems has a dominantly large fraction of harder events.

Similar studies are reported in Refs. [23,77], where the moderate increase of $\langle p_T \rangle$ in Pb-Pb collisions was related to collective flow. The strong increase of $\langle p_T \rangle$ with $\langle dN_{ch}/d\eta \rangle_{|\eta| < 0.5}$ in small collision systems can be further investigated by systematic studies of $\langle p_T \rangle$ from different models in pp and p -Pb collisions that incorporate processes like color reconnection, between strings produced in multiparton interactions, different string fragmentation processes and the core-corona mechanism. It was observed in Ref. [22] that the PYTHIA8 model with color reconnection, which introduces a flowlike effect, and the EPOS-LHC model, which uses parameterized flow, are able to reproduce the increasing trend of $\langle p_T \rangle$ as a function of multiplicity for K^{*0} and ϕ in pp collisions at $\sqrt{s} = 13$ TeV. The p -Pb measurements are important, as in Ref. [77] it is shown that the $\langle p_T \rangle$ of charged hadrons as a function of multiplicity shows a similar behavior as in pp collisions at low multiplicity, whereas it seems to approach a similar but less prominent trend of saturation as in Pb-Pb collisions at high multiplicity.

The model comparison with p -Pb data shows that EPOS-LHC describes the increasing trend of $\langle p_T \rangle$ with multiplicity

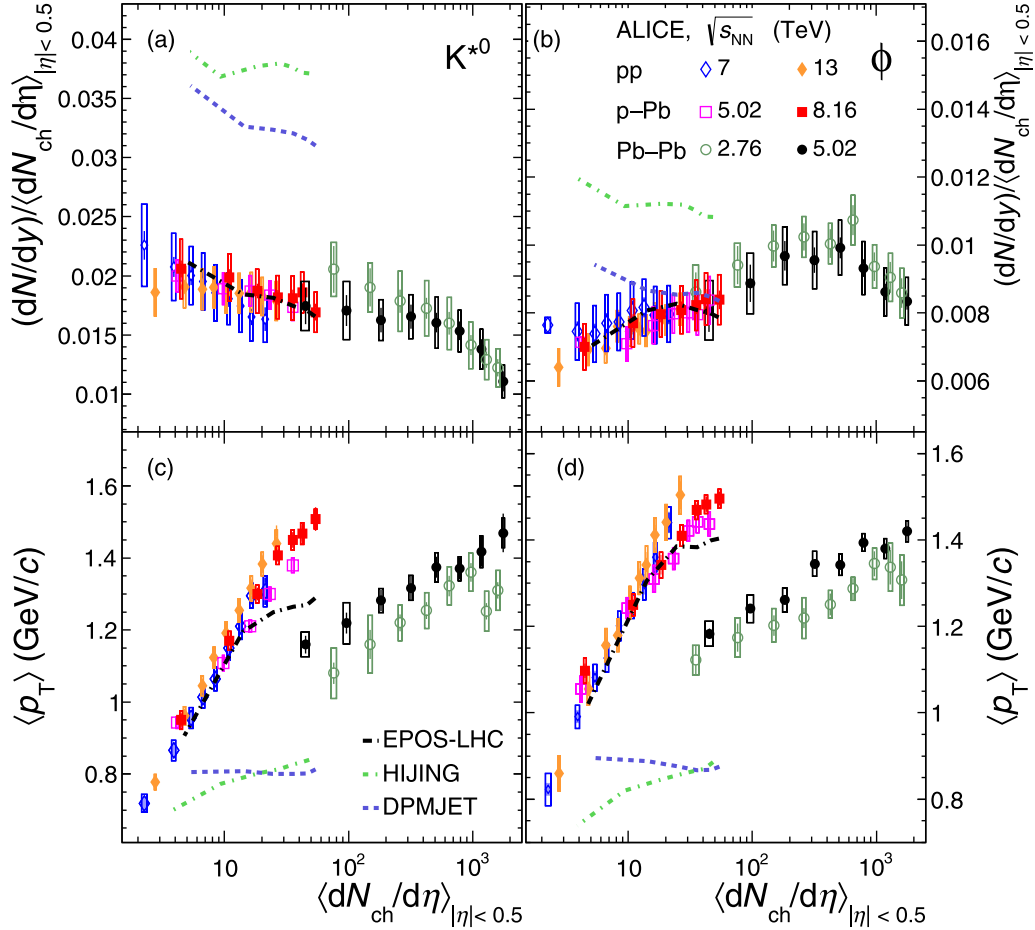


FIG. 5. The multiplicity-scaled integrated yield $((dN/dy)/\langle dN_{ch}/d\eta \rangle_{|\eta|<0.5})$ (upper panels) and mean transverse momentum $(\langle p_T \rangle)$ (bottom panels) for K^{*0} (left panels) and ϕ (right panels) as a function of $\langle dN_{ch}/d\eta \rangle_{|\eta|<0.5}$ measured in the ALICE central barrel in pp collisions at $\sqrt{s} = 7, 13$ TeV, in p -Pb collisions at $\sqrt{s_{NN}} = 5.02, 8.16$ TeV, and Pb-Pb collisions at $\sqrt{s_{NN}} = 2.76, 5.02$ TeV. Measurements are compared with the predictions from EPOS-LHC [31,69], DPMJET [32], and HIJING [33] for p -Pb collisions at $\sqrt{s_{NN}} = 8.16$ TeV. Statistical uncertainties are represented as bars, boxes indicate total systematic uncertainties.

for both K^{*0} and ϕ , and it gives a better agreement for ϕ to high multiplicity values. DPMJET and HIJING models fail to describe the observed trend in $\langle p_T \rangle$ for both K^{*0} and ϕ and underpredict the data for all multiplicities.

C. x_T scaling

Particle invariant production cross-sections are known to follow a scaling in the measurement of the transverse momentum spectrum for different collision energies at high p_T using the scaling variable $x_T = 2p_T/\sqrt{s}$ [39,40]. The x_T scaling was tested in pp collisions for identified hadrons in STAR [45], ALICE [46], and for (nonidentified) charged particles in CDF [41–43], UA1 [44], and CMS [47]. In this paper, the validity of empirical x_T scaling is tested using the K^{*0} and ϕ measurements in p -Pb collisions at $\sqrt{s_{NN}} = 8.16$ TeV reported here and those obtained at $\sqrt{s_{NN}} = 5.02$ TeV [23]. The invariant cross-sections are determined from the measured invariant yield as $Ed^3\sigma/dp^3 = \sigma_{inel} \times Ed^3N/dp^3$, where $\sigma_{inel} = (72.5 \pm 0.5)$ mb and (67.6 ± 0.6) mb is the inelastic

cross-section in pp collisions at $\sqrt{s} = 8.16$ and 5.02 TeV, respectively [78].

At fixed x_T , the invariant cross-section $Ed^3\sigma/dp^3$ scales as p_T^{-n} , where the exponent of scaling n depends on x_T and $\sqrt{s_{NN}}$, and is calculated using the following equation:

$$n(x_T, \sqrt{s_{NN1}}, \sqrt{s_{NN2}}) = \frac{\ln(\sigma^{inv}(x_T, \sqrt{s_{NN2}})/\sigma^{inv}(x_T, \sqrt{s_{NN1}}))}{\ln(\sqrt{s_{NN1}}/\sqrt{s_{NN2}})}, \quad (1)$$

where $x_T = 2p_T/\sqrt{s_{NN}}$. The distributions of n values as a function of x_T for K^{*0} and ϕ are shown in Fig. 6. In the low x_T region, where the particle production is dominated by soft processes, the values of n are found to increase with x_T , whereas the n values seem to saturate at high x_T . The n values are obtained by fitting the $n(x_T, \sqrt{s_{NN}})$ distribution by a constant function in the x_T range $1.3 \times 10^{-3} < x_T < 4 \times 10^{-3}$ for both K^{*0} and ϕ . The x_T spectra for both particles are scaled by the corresponding $(\sqrt{s_{NN}}/\text{GeV})^n$. The best scaling

TABLE III. The values of dN/dy and $\langle p_T \rangle$ are presented for different multiplicity classes in p -Pb collisions at $\sqrt{s_{NN}} = 8.16$ TeV. In each entry, the first uncertainty is statistical and the second is systematic. The value given in the parentheses corresponds to uncorrelated part of the systematic uncertainty. The fraction of total yield obtained by extrapolation (“extr.”) are also reported.

K^{*0}			
Multiplicity (%)	extr.	dN/dy	$\langle p_T \rangle$ (GeV/c)
0–5	–	$0.913 \pm 0.030 \pm 0.086$ (0.047)	$1.509 \pm 0.033 \pm 0.028$ (0.018)
5–10	–	$0.783 \pm 0.025 \pm 0.074$ (0.050)	$1.461 \pm 0.029 \pm 0.030$ (0.021)
10–20	–	$0.644 \pm 0.015 \pm 0.060$ (0.047)	$1.460 \pm 0.021 \pm 0.028$ (0.020)
20–40	–	$0.489 \pm 0.009 \pm 0.045$ (0.028)	$1.407 \pm 0.016 \pm 0.025$ (0.017)
40–60	–	$0.344 \pm 0.006 \pm 0.032$ (0.018)	$1.301 \pm 0.014 \pm 0.025$ (0.014)
60–80	–	$0.220 \pm 0.004 \pm 0.020$ (0.016)	$1.176 \pm 0.012 \pm 0.026$ (0.020)
80–100	–	$0.092 \pm 0.002 \pm 0.008$ (0.006)	$0.950 \pm 0.011 \pm 0.026$ (0.018)
NSD	–	$0.396 \pm 0.004 \pm 0.037$	$1.335 \pm 0.008 \pm 0.027$
ϕ			
Multiplicity (%)	extr.	dN/dy	$\langle p_T \rangle$ (GeV/c)
0–5	0.089	$0.455 \pm 0.008 \pm 0.041$ (0.026)	$1.496 \pm 0.015 \pm 0.022$ (0.021)
5–10	0.088	$0.356 \pm 0.007 \pm 0.033$ (0.028)	$1.482 \pm 0.017 \pm 0.022$ (0.021)
10–20	0.093	$0.292 \pm 0.004 \pm 0.028$ (0.018)	$1.468 \pm 0.013 \pm 0.021$ (0.016)
20–40	0.101	$0.217 \pm 0.003 \pm 0.020$ (0.008)	$1.409 \pm 0.011 \pm 0.025$ (0.010)
40–60	0.104	$0.146 \pm 0.002 \pm 0.014$ (0.007)	$1.342 \pm 0.011 \pm 0.029$ (0.021)
60–80	0.122	$0.084 \pm 0.001 \pm 0.008$ (0.004)	$1.249 \pm 0.013 \pm 0.025$ (0.020)
80–100	0.141	$0.0313 \pm 0.0008 \pm 0.003$ (0.002)	$1.097 \pm 0.016 \pm 0.029$ (0.008)
NSD	0.103	$0.161 \pm 0.002 \pm 0.015$	$1.393 \pm 0.008 \pm 0.024$

is obtained in the quoted fitting range with an exponent of $n = 4.94 \pm 0.10$ (sys.) for K^{*0} and $n = 5.12 \pm 0.07$ (sys.) for ϕ . The systematic uncertainties on the exponent n are calculated by changing the fit range in $n(x_T, \sqrt{s_{NN}})$ versus x_T distribution. The maximum deviation of n value with respect to the default one is taken as systematic uncertainties. The n values for K^{*0} and ϕ are consistent within the uncertainties, which suggests that the ratios of particle spectra attain similar values in p -Pb collisions at LHC energies. The x_T -scaled spectra for K^{*0} (left panel) and ϕ (right panel) in p -Pb collisions at $\sqrt{s_{NN}} = 5.02$ and 8.16 TeV are shown in Fig. 7.

These measurements suggest that the K^{*0} and ϕ yields in p -Pb collisions at LHC energies follow x_T scaling for $x_T \gtrsim 10^{-3}$. Similar studies were performed in pp collisions at LHC energies for identified hadrons (π^\pm , K^\pm , p (\bar{p}), and K^{*0}) with ALICE [46] and for charged hadrons with CMS [47]. The n values obtained in pp collisions for all hadron species except the proton are comparable to those reported here for K^{*0} and ϕ in p -Pb collisions. In Ref. [46], the proton takes a larger value of the exponent n , which was discussed in the context of the decrease of the baryon-to-meson ratio with increasing p_T in contrast to the nearly constant behavior of meson-to-meson ratios. The n value obtained at LHC energies is also observed to be lower than at RHIC energies, which suggests an increasing contribution of hard processes at higher center-of-mass energies.

A combined fit to the scaled differential cross-sections of K^{*0} and ϕ is performed with a power-law function of the form $a \times x_T^b \times (1+x_T)^c$ to verify the quality of the scaling behavior. Here, a , b , and c are free parameters. The fitting is done in

the region above $x_T \gtrsim 1.3 \times 10^{-3}$ (shown as black curve in Fig. 7), where the x_T scaling is observed. The χ^2/ndf value for K^{*0} (ϕ) is 0.16 (0.6), which confirms the good quality of the fit. In the fitting region, the measurements agree with the combined power-law fits within $\approx 20\%$ for both K^{*0} and ϕ . The measurements at $\sqrt{s_{NN}} = 8.16$ TeV are consistent, over the accessible x_T range $1.3 \times 10^{-3} < x_T < 3 \times 10^{-3}$, with empirical x_T scaling and with measurements from p -Pb collisions at $\sqrt{s_{NN}} = 5.02$ TeV. This further helps understanding and

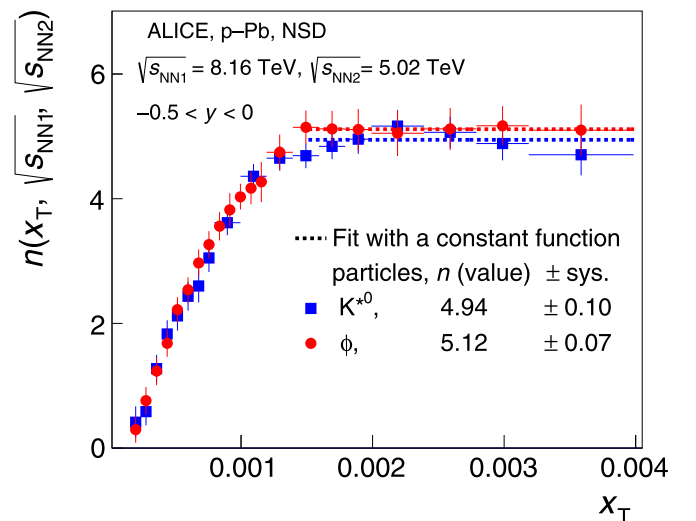


FIG. 6. The values of n as a function of x_T for K^{*0} and ϕ in p -Pb collisions.

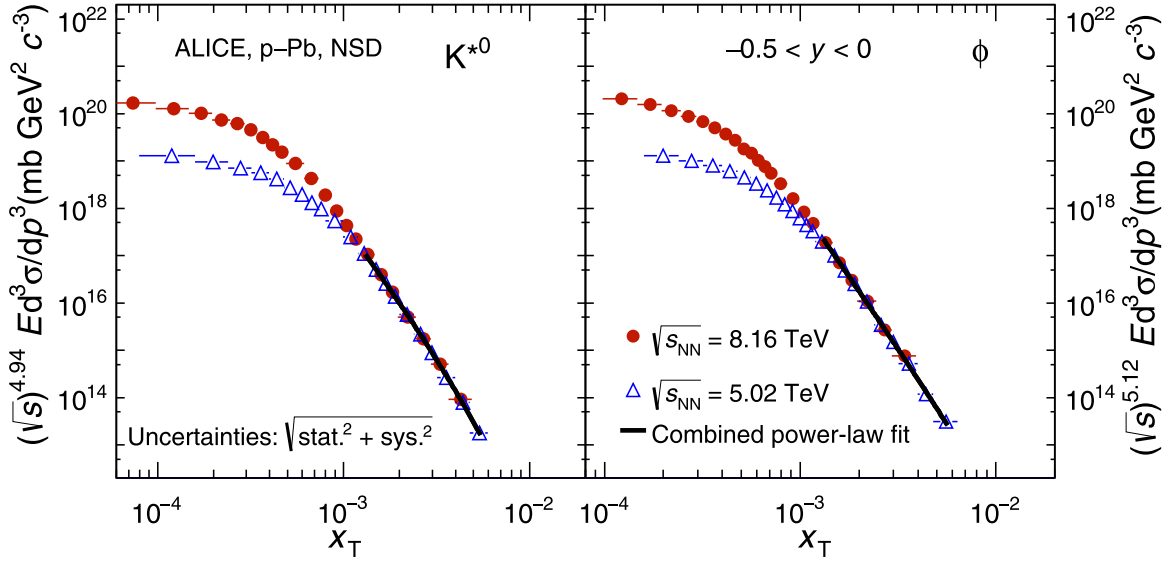


FIG. 7. Scaled invariant yield of K^{*0} and ϕ as a function of $x_T = 2p_T/\sqrt{s_{NN}}$ in p -Pb collisions at different energies $\sqrt{s_{NN}} = 5.02$ and 8.16 TeV.

distinguishing the contributions of the soft and hard processes to particle production.

D. Nuclear modification factor (R_{pPb})

To understand the nuclear effects, the nuclear modification factor (R_{pPb}) is an important observable in p -Pb collisions. It is calculated as

$$R_{pPb}(p_T) = \frac{d^2 N_{pPb}/dp_T dy}{\langle T_{pPb} \rangle d^2 \sigma_{pp}^{INEL}/dp_T dy}, \quad (2)$$

where $d^2 N_{pPb}/dp_T dy$ is the yield in p -Pb collisions and $d^2 \sigma_{pp}^{INEL}/dp_T dy$ is the invariant cross-section in inelastic pp collisions. $\langle T_{pPb} \rangle = \langle N_{coll} \rangle / \sigma^{INEL}$ is the average nuclear overlap function, which accounts for the nuclear collision geometry as obtained from a Glauber model [78]. If the nuclear modification factor is unity, then the yield in nuclear collisions is the same as from an incoherent superposition of nucleon-nucleon collisions.

In the absence of K^{*0} and ϕ measurements in pp collisions at $\sqrt{s} = 8.16$ TeV, the reference p_T spectra are obtained from the distributions measured in pp collisions at $\sqrt{s} = 8$ TeV [21] scaled by the ratio between the p_T spectra at the two energies as obtained from PYTHIA 8.230 [52]. For the systematic study the reference pp spectra are also obtained using the measured p_T spectrum at $\sqrt{s} = 7$ TeV [16]. The total systematic uncertainty of the pp reference spectrum is then calculated as the quadrature sum of the systematic uncertainties of the measured p_T spectrum at $\sqrt{s} = 8$ TeV and the difference of the reference spectra obtained using the measured p_T spectra at $\sqrt{s} = 7$ and 8 TeV. The systematic uncertainties of the reference p_T spectra of K^{*0} (ϕ) are 11.5% (7.3%) for the low p_T (<4 GeV/c) and 15.5% (7.4%) for the high p_T (>4 GeV/c) [26]. The systematic and statistical uncertainties of R_{pPb} are calculated as the quadrature sum of respective uncertainties of the p_T spectra in p -Pb

and pp collisions. The value of the nucleon–nucleon inelastic cross-section for the reference spectra at $\sqrt{s} = 8.16$ TeV is (72.5 ± 0.5) mb, taken from Ref. [78].

The R_{pPb} measurements of K^{*0} , ϕ , and multistrange baryon (Ξ and Ω) in p -Pb collisions at $\sqrt{s_{NN}} = 5.02$ TeV are also reported here. The R_{pPb} of K^{*0} and ϕ at $\sqrt{s_{NN}} = 5.02$ TeV are calculated from the measured p_T spectra in pp and p -Pb collisions published in Refs. [18,19,23]. The p_T spectra measurements of multistrange baryon (Ξ and Ω) production in p -Pb collisions are reported in Ref. [27]. Due to the unavailability of multistrange baryon measurements in pp collisions at $\sqrt{s} = 5.02$ TeV, reference p_T spectra are calculated by interpolating the measurements at $\sqrt{s} = 2.76$ [79] and 7 TeV [80], in each p_T interval, assuming a power-law dependence as a function of \sqrt{s} . The systematic uncertainties of the reference p_T spectra are taken as the maximum relative systematic uncertainty of the measured p_T spectra at $\sqrt{s} = 2.76$ and 7 TeV. This approach is similar to the one as described in Ref. [26] to obtain reference p_T spectra for π^\pm , K^\pm and $p(\bar{p})$ in pp collisions at $\sqrt{s} = 5.02$ TeV. Figure 8 shows the nuclear modification factor of K^{*0} (left panel) and ϕ (right panel) as a function of p_T in p -Pb collisions at $\sqrt{s_{NN}} = 5.02$ and 8.16 TeV. At intermediate p_T (2–8 GeV/c), there is a hint of increase in R_{pPb} , above unity which is more pronounced for K^{*0} than for ϕ . The measurements are consistent with each other within uncertainties. No significant energy dependence of R_{pPb} is observed for resonances in p -Pb collisions at the LHC energies.

Figure 9 shows the particle species dependence of the nuclear modification factors in p -Pb collisions at $\sqrt{s_{NN}} = 5.02$ and 8.16 TeV. Figures 9(a) and 9(b) show R_{pPb} of K^{*0} and ϕ at $\sqrt{s_{NN}} = 8.16$ and 5.02 TeV, respectively. Previous measurements of π and K mesons at $\sqrt{s_{NN}} = 5.02$ TeV [26] are also shown in Fig. 9(b). Figure 9(c) shows the R_{pPb} of multistrange baryons (Ξ , Ω) at $\sqrt{s_{NN}} = 5.02$ TeV. To study the mass dependence of baryons and to compare baryons and mesons,

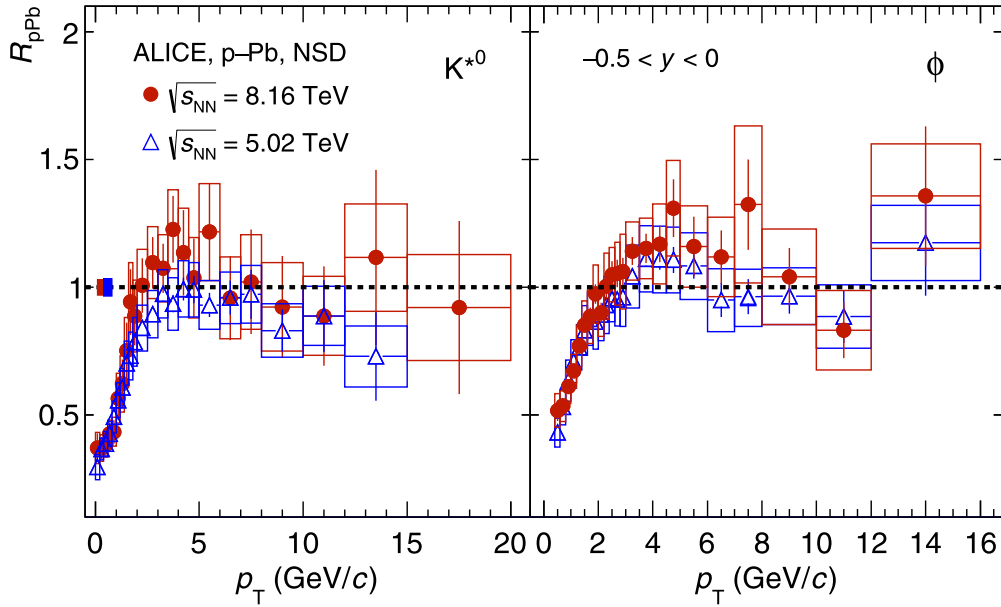


FIG. 8. Nuclear modification factor of K^{*0} and ϕ as a function of p_T in p -Pb collisions at different energies $\sqrt{s_{NN}} = 5.02$ and 8.16 TeV. The statistical and systematic uncertainties are represented by vertical bars and boxes, respectively. The normalization uncertainties are shown in each panel as boxes around $R_{pPb} = 1$ near $p_T = 0$ GeV/c.

the R_{pPb} of protons taken from Ref. [26] and that of ϕ mesons are also shown in Fig. 9(c). At low p_T (< 2 GeV/c), the R_{pPb} is less than unity for all hadrons. The measurements of K^{*0} and ϕ at $\sqrt{s_{NN}} = 5.02$ and 8.16 TeV are consistent with each other within uncertainties, no flavor dependence in R_{pPb} is observed. At intermediate p_T (2–8 GeV/c), the R_{pPb} of baryons shows a Cronin-like enhancement above unity [56]. The R_{pPb} shows a mass ordering and larger values are observed for the baryons

with higher masses. A similar mass ordering for baryons in this p_T region is also reported by CMS in Ref. [49] and the results are consistent with a hydrodynamical expectation of the radial flow [31]. It is also observed that the R_{pPb} of ϕ meson is smaller than that of the proton in spite of their similar masses, which may indicate baryon-meson ordering. Therefore, along with the presence of a strong radial flow component, there are other effects like different production

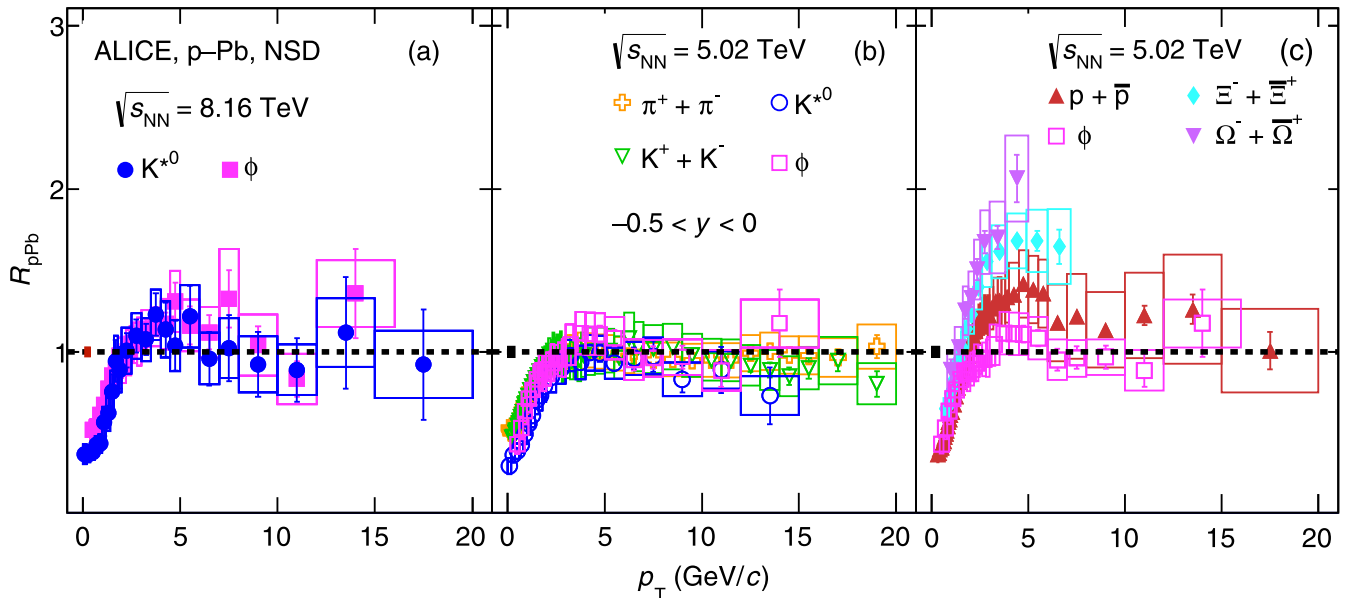


FIG. 9. The nuclear modification factor R_{pPb} as a function of transverse momentum p_T for different particle species in p -Pb collisions at $\sqrt{s_{NN}} = 5.02$ and 8.16 TeV. For comparison the results for π , K , and p [26] are also shown. The statistical and systematic uncertainties are represented by vertical bars and boxes, respectively. The normalization uncertainties are shown in each panel as boxes around $R_{pPb} = 1$ near $p_T = 0$ GeV/c.

mechanism for baryons and mesons which affect the R_{pPb} in this p_T region. Similar behavior is also observed in Pb-Pb collisions in this p_T region [36]. At high p_T (>8 GeV/c), the R_{pPb} values of all particles are consistent with unity within the uncertainties in p -Pb collisions at $\sqrt{s_{NN}} = 5.02$ and 8.16 TeV which suggests that there is no modification in R_{pPb} due to cold-nuclear matter effects for different particle species. Similar findings are also reported for π^0 meson with p_T up to 200 GeV/c in p -Pb collisions at $\sqrt{s_{NN}} = 8.16$ TeV [53], for charged hadrons in p -Pb collisions at $\sqrt{s_{NN}} = 5.02$ TeV by ALICE [26,48], and for strange hadrons by CMS in p -Pb collisions at $\sqrt{s_{NN}} = 5.02$ TeV [49] and by STAR in d -Au collisions at $\sqrt{s_{NN}} = 200$ GeV [25].

IV. SUMMARY

The production of K^{*0} and ϕ mesons as a function of p_T has been measured in the rapidity interval $-0.5 < y < 0$ for various multiplicity classes in p -Pb collisions at $\sqrt{s_{NN}} = 8.16$ TeV with the ALICE detector. The EPOS-LHC model describes the NSD p_T distribution while the DPMJET and HIJING models largely overestimate the distribution at low p_T . A significant evolution of spectral shapes with multiplicity is observed for $p_T < 4$ GeV/c, with a pattern similar to that of Pb-Pb collisions, which can be attributed to the collective radial expansion of the system. The spectral shapes are similar for all multiplicity classes at high p_T . The scaled p_T -integrated yields $[(dN/dy)/(\langle dN_{ch}/d\eta \rangle_{|\eta|<0.5})]$ as a function of multiplicity show a smooth evolution from small systems, pp and p -Pb, to Pb-Pb, and the values are similar for a given multiplicity, irrespective of the colliding systems and energies, suggesting that the hadrochemistry at LHC energies is mainly driven by the event multiplicity. The $\langle p_T \rangle$ values of K^{*0} and ϕ increase as a function of multiplicity and follow a different trend in p -Pb and pp than Pb-Pb collisions. The EPOS-LHC model which includes parameterized flow gives a good quantitative description of the scaled p_T -integrated yields and describes qualitatively the increase in $\langle p_T \rangle$ values with multiplicity for both K^{*0} and ϕ . An empirical x_T scaling for K^{*0} and ϕ holds (within roughly 20%) in the hard scattering region of the particle production. The obtained value of the exponent ($n \approx 5$) is lower than at RHIC energies which suggests an increasing contribution of hard scattering processes at higher $\sqrt{s_{NN}}$. Furthermore, the value of the exponent n in p -Pb collisions is compatible with those in pp collisions for π^\pm , K^\pm and K^{*0} suggesting that the high- p_T particle production mechanism is similar in both collision systems. No significant energy dependence in R_{pPb} is observed for K^{*0} and ϕ in p -Pb collisions at $\sqrt{s_{NN}} = 5.02$ and 8.16 TeV. At intermediate p_T ($2 < p_T < 8$ GeV/c), R_{pPb} values for multistrange baryon (Ξ and Ω) and the protons in p -Pb collisions at $\sqrt{s_{NN}} = 5.02$ TeV show a Cronin-like enhancement and the values are found to be significantly larger than those for π^\pm , K^\pm , K^{*0} , and ϕ . The R_{pPb} values are consistent with unity within the uncertainties for all species at $p_T > 8$ GeV/c, which further confirms the absence of cold-nuclear matter effects in this p_T range. Future measurements of light flavor hadron (π^\pm , K^\pm , $p(\bar{p})$ etc.) yields up to high p_T in p -Pb collisions at $\sqrt{s_{NN}} = 8.16$ TeV are

required for a comprehensive study of nuclear modification factor and x_T scaling.

ACKNOWLEDGMENTS

The ALICE Collaboration thanks all its engineers and technicians for their invaluable contributions to the construction of the experiment and the CERN accelerator teams for the outstanding performance of the LHC complex. The ALICE Collaboration gratefully acknowledges the resources and support provided by all Grid centers and the Worldwide LHC Computing Grid (WLCG) collaboration. The ALICE Collaboration acknowledges the following funding agencies for their support in building and running the ALICE detector: A. I. Alikhanyan National Science Laboratory (Yerevan Physics Institute) Foundation (ANSL), State Committee of Science and World Federation of Scientists (WFS), Armenia; Austrian Academy of Sciences, Austrian Science Fund (FWF): [M 2467-N36] and Nationalstiftung für Forschung, Technologie und Entwicklung, Austria; Ministry of Communications and High Technologies, National Nuclear Research Center, Azerbaijan; Conselho Nacional de Desenvolvimento Científico e Tecnológico (CNPq), Financiadora de Estudos e Projetos (Finep), Fundação de Amparo à Pesquisa do Estado de São Paulo (FAPESP) and Universidade Federal do Rio Grande do Sul (UFRGS), Brazil; Ministry of Education of China (MOEC), Ministry of Science & Technology of China (MSTC) and National Natural Science Foundation of China (NSFC), China; Ministry of Science and Education and Croatian Science Foundation, Croatia; Centro de Aplicaciones Tecnológicas y Desarrollo Nuclear (CEADEN), Cubaenergía, Cuba; Ministry of Education, Youth and Sports of the Czech Republic, Czech Republic; The Danish Council for Independent Research—Natural Sciences, the VILLUM FONDEN and Danish National Research Foundation (DNRF), Denmark; Helsinki Institute of Physics (HIP), Finland; Commissariat à l’Energie Atomique (CEA) and Institut National de Physique Nucléaire et de Physique des Particules (IN2P3) and Centre National de la Recherche Scientifique (CNRS), France; Bundesministerium für Bildung und Forschung (BMBF) and GSI Helmholtzzentrum für Schwerionenforschung GmbH, Germany; General Secretariat for Research and Technology, Ministry of Education, Research and Religions, Greece; National Research, Development and Innovation Office, Hungary; Department of Atomic Energy Government of India (DAE), Department of Science and Technology, Government of India (DST), University Grants Commission, Government of India (UGC) and Council of Scientific and Industrial Research (CSIR), India; Indonesian Institute of Science, Indonesia; Istituto Nazionale di Fisica Nucleare (INFN), Italy; Japanese Ministry of Education, Culture, Sports, Science and Technology (MEXT), Japan Society for the Promotion of Science (JSPS) KAKENHI and Japanese Ministry of Education, Culture, Sports, Science and Technology (MEXT) of Applied Science (IIST), Japan; Consejo Nacional de Ciencia (CONACYT) y Tecnología, through Fondo de Cooperación Internacional en Ciencia y Tecnología (FONCICYT) and Dirección General de Asuntos del Personal Académico (DGAPA), Mexico;

Nederlandse Organisatie voor Wetenschappelijk Onderzoek (NWO), Netherlands; The Research Council of Norway, Norway; Commission on Science and Technology for Sustainable Development in the South (COMSATS), Pakistan; Pontificia Universidad Católica del Perú, Peru; Ministry of Education and Science, National Science Centre and WUT ID-UB, Poland; Korea Institute of Science and Technology Information and National Research Foundation of Korea (NRF), Republic of Korea; Ministry of Education and Scientific Research, Institute of Atomic Physics and Ministry of Research and Innovation and Institute of Atomic Physics, Romania; Joint Institute for Nuclear Research (JINR), Ministry of Education and Science of the Russian Federation, National Research Centre Kurchatov Institute, Russian Science Foundation and Russian Foundation for Basic Research, Russia;

Ministry of Education, Science, Research and Sport of the Slovak Republic, Slovakia; National Research Foundation of South Africa, South Africa; Swedish Research Council (VR) and Knut & Alice Wallenberg Foundation (KAW), Sweden; European Organization for Nuclear Research, Switzerland; Suranaree University of Technology (SUT), National Science and Technology Development Agency (NSDTA) and Office of the Higher Education Commission under NRU project of Thailand, Thailand; Turkish Energy, Nuclear and Mineral Research Agency (TENMAK), Turkey; National Academy of Sciences of Ukraine, Ukraine; Science and Technology Facilities Council (STFC), United Kingdom; National Science Foundation of the United States of America (NSF) and United States Department of Energy, Office of Nuclear Physics (DOE NP), United States of America.

-
- [1] P. Braun-Munzinger, V. Koch, T. Schäfer, and J. Stachel, Properties of hot and dense matter from relativistic heavy ion collisions, *Phys. Rep.* **621**, 76 (2016).
- [2] J. Adams *et al.* (STAR Collaboration), Experimental and theoretical challenges in the search for the quark gluon plasma: The STAR Collaboration's critical assessment of the evidence from RHIC collisions, *Nucl. Phys. A* **757**, 102 (2005).
- [3] J. Schukraft (ALICE Collaboration), Heavy-ion physics with the ALICE experiment at the CERN Large Hadron Collider, *Philos. Trans. R. Soc. London A* **370**, 917 (2012).
- [4] M. M. Aggarwal *et al.* (STAR Collaboration), K^{*0} production in Cu+Cu and Au+Au collisions at $\sqrt{s_{NN}} = 62.4$ GeV and 200 GeV, *Phys. Rev. C* **84**, 034909 (2011).
- [5] J. Adams *et al.* (STAR Collaboration), $K^{*}(892)^0$ resonance production in Au+Au and p+p collisions at $\sqrt{s_{NN}} = 200$ GeV at STAR, *Phys. Rev. C* **71**, 064902 (2005).
- [6] C. Adler *et al.* (STAR Collaboration), $K^{*}(892)^0$ production in relativistic heavy ion collisions at $\sqrt{s_{NN}} = 130$ GeV, *Phys. Rev. C* **66**, 061901 (2002).
- [7] T. Anticic *et al.* (NA49 Collaboration), $K^{*}(892)^0$ and $\bar{K}^{*}(892)^0$ production in central Pb+Pb, Si+Si, C+C, and inelastic p+p collisions at 158A GeV, *Phys. Rev. C* **84**, 064909 (2011).
- [8] B. I. Abelev *et al.* (STAR Collaboration), Energy and system size dependence of ϕ meson production in Cu+Cu and Au+Au collisions, *Phys. Lett. B* **673**, 183 (2009).
- [9] B. I. Abelev *et al.* (STAR Collaboration), Measurements of ϕ meson production in relativistic heavy-ion collisions at RHIC, *Phys. Rev. C* **79**, 064903 (2009).
- [10] L. Adamczyk *et al.* (STAR Collaboration), Probing parton dynamics of QCD matter with Ω and ϕ production, *Phys. Rev. C* **93**, 021903 (2016).
- [11] C. Alt *et al.* (NA49 Collaboration), Energy dependence of ϕ meson production in central Pb+Pb collisions at $\sqrt{s_{NN}} = 6$ to 17 GeV, *Phys. Rev. C* **78**, 044907 (2008).
- [12] A. Adare *et al.* (PHENIX Collaboration), Nuclear modification factors of ϕ mesons in d+Au, Cu+Cu, and Au+Au collisions at $\sqrt{s_{NN}} = 200$ GeV, *Phys. Rev. C* **83**, 024909 (2011).
- [13] B. Abelev *et al.* (ALICE Collaboration), $K^{*}(892)^0$ and $\phi(1020)$ production in Pb-Pb collisions at $\sqrt{s_{NN}} = 2.76$ TeV, *Phys. Rev. C* **91**, 024609 (2015).
- [14] A. Adare *et al.* (PHENIX Collaboration), Measurement of K^{*0} in p + p, d+Au, and Cu+Cu collisions at $\sqrt{s_{NN}} = 200$ GeV, *Phys. Rev. C* **90**, 054905 (2014).
- [15] J. Adam *et al.* (ALICE Collaboration), $K^{*}(892)^0$ and $\phi(1020)$ meson production at high transverse momentum in pp and Pb-Pb collisions at $\sqrt{s_{NN}} = 2.76$ TeV, *Phys. Rev. C* **95**, 064606 (2017).
- [16] B. Abelev *et al.* (ALICE Collaboration), Production of $K^{*}(892)^0$ and $\phi(1020)$ in pp collisions at $\sqrt{s} = 7$ TeV, *Eur. Phys. J. C* **72**, 2183 (2012).
- [17] J. Adam *et al.* (ALICE Collaboration), Enhanced production of multistrange hadrons in high-multiplicity proton-proton collisions, *Nat. Phys.* **13**, 535 (2017).
- [18] S. Acharya *et al.* (ALICE Collaboration), Evidence of rescattering effect in Pb-Pb collisions at the LHC through production of $K^{*}(892)^0$ and $\phi(1020)$ mesons, *Phys. Lett. B* **802**, 135225 (2020).
- [19] S. Acharya *et al.* (ALICE Collaboration), Production of $K^{*}(892)^0$ and $\phi(1020)$ in pp and Pb-Pb collisions at $\sqrt{s_{NN}} = 5.02$ TeV, *Phys. Rev. C* **106**, 034907 (2022).
- [20] S. Acharya *et al.* (ALICE Collaboration), Multiplicity dependence of light-flavor hadron production in pp collisions at $\sqrt{s} = 7$ TeV, *Phys. Rev. C* **99**, 024906 (2019).
- [21] S. Acharya *et al.* (ALICE Collaboration), $K^{*}(892)^0$ and $\phi(1020)$ production at midrapidity in pp collisions at $\sqrt{s} = 8$ TeV, *Phys. Rev. C* **102**, 024912 (2020).
- [22] S. Acharya *et al.* (ALICE Collaboration), Multiplicity dependence of $K^{*}(892)^0$ and $\phi(1020)$ production in pp collisions at $\sqrt{s} = 13$ TeV, *Phys. Lett. B* **807**, 135501 (2020).
- [23] J. Adam *et al.* (ALICE Collaboration), Production of $K^{*}(892)^0$ and $\phi(1020)$ in p-Pb collisions at $\sqrt{s_{NN}} = 5.02$ TeV, *Eur. Phys. J. C* **76**, 245 (2016).
- [24] B. Abelev *et al.* (ALICE Collaboration), Transverse sphericity of primary charged particles in minimum bias proton-proton collisions at $\sqrt{s} = 0.9, 2.76,$ and 7 TeV, *Eur. Phys. J. C* **72**, 2124 (2012).
- [25] B. I. Abelev *et al.* (STAR Collaboration), Hadronic resonance production in d+Au collisions at $\sqrt{s_{NN}} = 200$ GeV at RHIC, *Phys. Rev. C* **78**, 044906 (2008).
- [26] J. Adam *et al.* (ALICE Collaboration), Multiplicity dependence of charged pion, kaon, and (anti)proton production at large

- transverse momentum in p -Pb collisions at $\sqrt{s_{NN}} = 5.02$ TeV, *Phys. Lett. B* **760**, 720 (2016).
- [27] J. Adam *et al.* (ALICE Collaboration), Multi-strange baryon production in p -Pb collisions at $\sqrt{s_{NN}} = 5.02$ TeV, *Phys. Lett. B* **758**, 389 (2016).
- [28] S. Acharya *et al.* (ALICE Collaboration), Measurement of $\Lambda(1520)$ production in pp collisions at $\sqrt{s} = 7$ TeV and p -Pb collisions at $\sqrt{s_{NN}} = 5.02$ TeV, *Eur. Phys. J. C* **80**, 160 (2020).
- [29] D. Adamova *et al.* (ALICE Collaboration), Production of $\Sigma(1385)^\pm$ and $\Xi(1530)^0$ in p -Pb collisions at $\sqrt{s_{NN}} = 5.02$ TeV, *Eur. Phys. J. C* **77**, 389 (2017).
- [30] B. B. Abelev *et al.* (ALICE Collaboration), Production of $\Sigma(1385)^\pm$ and $\Xi(1530)^0$ in proton-proton collisions at $\sqrt{s} = 7$ TeV, *Eur. Phys. J. C* **75**, 1 (2015).
- [31] T. Pierog, I. Karpenko, J. M. Katzy, E. Yatsenko, and K. Werner, EPOS LHC: Test of collective hadronization with data measured at the CERN Large Hadron Collider, *Phys. Rev. C* **92**, 034906 (2015).
- [32] S. Roesler, R. Engel, and J. Ranft, The Monte Carlo event generator DPMJET-III, in *Advanced Monte Carlo for Radiation Physics, Particle Transport Simulation and Applications*, edited by A. Kling, F. J. C. Barão, M. Nakagawa, L. Távora, and P. Vaz (Springer, Berlin, Heidelberg, 2001), pp. 1033–1038.
- [33] M. Gyulassy and X.-N. Wang, HIJING 1.0: A Monte Carlo program for parton and particle production in high-energy hadronic and nuclear collisions, *Comput. Phys. Commun.* **83**, 307 (1994).
- [34] S. Acharya *et al.* (ALICE Collaboration), Multiplicity dependence of (multi)strange hadron production in proton-proton collisions at $\sqrt{s} = 13$ TeV, *Eur. Phys. J. C* **80**, 167 (2020).
- [35] B. Abelev *et al.* (ALICE Collaboration), Centrality dependence of π , K, p production in Pb-Pb collisions at $\sqrt{s_{NN}} = 2.76$ TeV, *Phys. Rev. C* **88**, 044910 (2013).
- [36] S. Acharya *et al.* (ALICE Collaboration), Production of charged pions, kaons, and (anti)protons in Pb-Pb and inelastic pp collisions at $\sqrt{s_{NN}} = 5.02$ TeV, *Phys. Rev. C* **101**, 044907 (2020).
- [37] J. C. Collins, D. E. Soper, and G. F. Sterman, Factorization of hard processes in QCD, *Adv. Ser. Direct. High Energy Phys.* **5**, 1 (1989).
- [38] D. de Florian, R. Sassot, M. Epele, R. J. Hernández-Pinto, and M. Stratmann, Parton-to-pion fragmentation reloaded, *Phys. Rev. D* **91**, 014035 (2015).
- [39] S. J. Brodsky, H. J. Pirner, and J. Raufeisen, Scaling properties of high p_T inclusive hadron production, *Phys. Lett. B* **637**, 58 (2006).
- [40] F. Arleo, S. J. Brodsky, D. S. Hwang, and A. M. Sickles, Higher-Twist Dynamics in Large Transverse Momentum Hadron Production, *Phys. Rev. Lett.* **105**, 062002 (2010).
- [41] T. Aaltonen *et al.* (CDF Collaboration), Measurement of particle production and inclusive differential cross sections in $p\bar{p}$ collisions at $\sqrt{s} = 1.96$ TeV, *Phys. Rev. D* **79**, 112005 (2009); **82**, 119903(E) (2010).
- [42] D. Acosta *et al.* (CDF Collaboration), Soft and hard interactions in $p\bar{p}$ collisions at $\sqrt{s} = 1800$ and 630 GeV, *Phys. Rev. D* **65**, 072005 (2002).
- [43] F. Abe *et al.* (CDF Collaboration), Transverse Momentum Distributions of Charged Particles Produced in $p\bar{p}$ Interactions at $\sqrt{s} = 630$ and 1800 GeV, *Phys. Rev. Lett.* **61**, 1819 (1988).
- [44] C. Albajar *et al.* (UA1 Collaboration), A study of the general characteristics of $p\bar{p}$ collisions at $\sqrt{s} = 0.2$ to 0.9 TeV, *Nucl. Phys. B* **335**, 261 (1990).
- [45] J. Adams *et al.* (STAR Collaboration), Identified hadron spectra at large transverse momentum in $p+p$ and $d+Au$ collisions at $\sqrt{s_{NN}} = 200$ GeV, *Phys. Lett. B* **637**, 161 (2006).
- [46] S. Acharya *et al.* (ALICE Collaboration), Production of light-flavor hadrons in pp collisions at $\sqrt{s} = 7$ and $\sqrt{s} = 13$ TeV, *Eur. Phys. J. C* **81**, 256 (2021).
- [47] S. Chatrchyan *et al.* (CMS Collaboration), Charged particle transverse momentum spectra in pp collisions at $\sqrt{s} = 0.9$ and 7 TeV, *J. High Energy Phys.* **08** (2011) 086.
- [48] S. Acharya *et al.* (ALICE Collaboration), Transverse momentum spectra and nuclear modification factors of charged particles in pp , p -Pb, and Pb-Pb collisions at the LHC, *J. High Energy Phys.* **11** (2018) 013.
- [49] A. M. Sirunyan *et al.* (CMS Collaboration), Strange hadron production in pp and pPb collisions at $\sqrt{s_{NN}} = 5.02$ TeV, *Phys. Rev. C* **101**, 064906 (2020).
- [50] V. Khachatryan *et al.* (CMS Collaboration), Multiplicity and rapidity dependence of strange hadron production in pp , pPb , and $PbPb$ collisions at the LHC, *Phys. Lett. B* **768**, 103 (2017).
- [51] B. B. Abelev *et al.* (ALICE Collaboration), Multiplicity Dependence of Pion, Kaon, Proton and lambda production in p -Pb collisions at $\sqrt{s_{NN}} = 5.02$ TeV, *Phys. Lett. B* **728**, 25 (2014).
- [52] T. Sjöstrand, S. Ask, J. R. Christiansen, R. Corke, N. Desai, P. Ilten, S. Mrenna, S. Prestel, C. O. Rasmussen, and P. Z. Skands, An introduction to PYTHIA 8.2, *Comput. Phys. Commun.* **191**, 159 (2015).
- [53] S. Acharya *et al.* (ALICE Collaboration), Nuclear modification factor of light neutral-meson spectra up to high transverse momentum in p -Pb collisions at $\sqrt{s_{NN}} = 8.16$ TeV, *Phys. Lett. B* **827**, 136943 (2022).
- [54] R. J. Fries, B. Muller, C. Nonaka, and S. A. Bass, Hadronization in Heavy-Ion Collisions: Recombination and Fragmentation of Partons, *Phys. Rev. Lett.* **90**, 202303 (2003).
- [55] Z.-B. Kang, I. Vitev, and H. Xing, Nuclear modification of high transverse momentum particle production in $p+A$ collisions at RHIC and LHC, *Phys. Lett. B* **718**, 482 (2012).
- [56] B. Z. Kopeliovich, J. Nemchik, A. Schafer, and A. V. Tarasov, Cronin Effect in Hadron Production off Nuclei, *Phys. Rev. Lett.* **88**, 232303 (2002).
- [57] J. W. Cronin, H. J. Frisch, M. J. Shochet, J. P. Boymond, P. A. Piroue, and R. L. Sumner, Production of Hadrons with Large Transverse Momentum at 200 and 300 GeV, *Phys. Rev. Lett.* **31**, 1426 (1973).
- [58] J. W. Cronin, H. J. Frisch, M. J. Shochet, J. P. Boymond, R. Mermod, P. A. Piroue, and R. L. Sumner, Production of hadrons with large transverse momentum at 200, 300, and 400 GeV, *Phys. Rev. D* **11**, 3105 (1975).
- [59] K. Aamodt *et al.* (ALICE Collaboration), The ALICE experiment at the CERN LHC, *JINST* **3**, S08002 (2008).
- [60] B. Abelev *et al.* (ALICE Collaboration), Performance of the ALICE experiment at the CERN LHC, *Int. J. Mod. Phys. A* **29**, 1430044 (2014).
- [61] E. Abbas *et al.* (ALICE Collaboration), Performance of the ALICE VZERO system, *J. Inst.* **8**, P10016 (2013).

- [62] S. Acharya *et al.* (ALICE Collaboration), Charged-particle pseudorapidity density at mid-rapidity in p -Pb collisions at $\sqrt{s_{NN}} = 8.16$ TeV, *Eur. Phys. J. C* **79**, 307 (2019).
- [63] K. Aamodt *et al.* (ALICE Collaboration), Alignment of the ALICE inner tracking system with cosmic-ray tracks, *JINST* **5**, P03003 (2010).
- [64] J. Alme *et al.*, The ALICE TPC, a large 3-dimensional tracking device with fast readout for ultra-high multiplicity events, *Nucl. Instrum. Methods Phys. Res., Sect. A* **622**, 316 (2010).
- [65] J. Adam *et al.* (ALICE Collaboration), Measurement of pion, kaon, and proton production in proton-proton collisions at $\sqrt{s} = 7$ TeV, *Eur. Phys. J. C* **75**, 226 (2015).
- [66] A. Akindinov *et al.*, Performance of the ALICE Time-Of-Flight detector at the LHC, *Eur. Phys. J. Plus* **128**, 44 (2013).
- [67] M. Tanabashi *et al.* (Particle Data Group Collaboration), Review of Particle Physics, *Phys. Rev. D* **98**, 030001 (2018).
- [68] R. Brun, F. Bruyant, M. Maire, A. C. McPherson, and P. Zancarini, GEANT 3: User's guide Geant 3.10, Geant 3.11; rev. version (CERN, Geneva, 1987), <https://cds.cern.ch/record/1119728>.
- [69] K. Werner, B. Guiot, I. Karpenko, and T. Pierog, Analyzing radial flow features in p -Pb and p - p collisions at several TeV by studying identified-particle production with the event generator EPOS3, *Phys. Rev. C* **89**, 064903 (2014).
- [70] K. Werner, I. Karpenko, M. Bleicher, and T. Pierog, The physics of EPOS, *EPJ Web Conf.* **52**, 05001 (2013).
- [71] H. J. Drescher, M. Hladik, S. Ostapchenko, T. Pierog, and K. Werner, Parton-based Gribov-Regge theory, *Phys. Rep.* **350**, 93 (2001).
- [72] K. Werner, Core-Corona Separation in Ultrarelativistic Heavy Ion Collisions, *Phys. Rev. Lett.* **98**, 152301 (2007).
- [73] T. Pierog and K. Werner, EPOS model and ultra high energy cosmic rays, *Nucl. Phys. B, Proc. Suppl.* **196**, 102 (2009).
- [74] K. Werner, I. Karpenko, T. Pierog, M. Bleicher, and K. Mikhailov, Event-by-event simulation of the three-dimensional hydrodynamic evolution from flux tube initial conditions in ultrarelativistic heavy ion collisions, *Phys. Rev. C* **82**, 044904 (2010).
- [75] S. Acharya *et al.* (ALICE Collaboration), Charged-particle production as a function of multiplicity and transverse sphericity in pp collisions at $\sqrt{s} = 5.02$ and 13 TeV, *Eur. Phys. J. C* **79**, 857 (2019).
- [76] C. Tsallis, Possible generalization of Boltzmann-Gibbs statistics, *J. Stat. Phys.* **52**, 479 (1988).
- [77] B. Abelev *et al.* (ALICE Collaboration), Multiplicity dependence of the average transverse momentum in pp , p -Pb, and Pb-Pb collisions at the LHC, *Phys. Lett. B* **727**, 371 (2013).
- [78] C. Loizides, J. Kamin, and D. d'Enterria, Improved Monte Carlo Glauber predictions at present and future nuclear colliders, *Phys. Rev. C* **97**, 054910 (2018); **99**, 019901(E) (2019).
- [79] B. Abelev *et al.* (ALICE Collaboration), Multi-strange baryon production at mid-rapidity in Pb-Pb collisions at $\sqrt{s_{NN}} = 2.76$ TeV, *Phys. Lett. B* **728**, 216 (2014); **734**, 314(E) (2014).
- [80] B. Abelev *et al.* (ALICE Collaboration), Multi-strange baryon production in pp collisions at $\sqrt{s} = 7$ TeV with ALICE, *Phys. Lett. B* **712**, 309 (2012).

S. Acharya,¹⁴² D. Adamová,⁹⁷ A. Adler,⁷⁵ J. Adolfsson,⁸² G. Aglieri Rinella,³⁴ M. Agnello,³⁰ N. Agrawal,⁵⁴ Z. Ahammed,¹⁴² S. Ahmad,¹⁶ S. U. Ahn,⁷⁷ I. Ahuja,³⁸ Z. Akbar,⁵¹ A. Akindinov,⁹⁴ M. Al-Turany,¹⁰⁹ S. N. Alam,¹⁶ D. Aleksandrov,⁹⁰ B. Alessandro,⁶⁰ H. M. Alfanda,⁷ R. Alfaro Molina,⁷² B. Ali,¹⁶ Y. Ali,¹⁴ A. Alici,²⁵ N. Alizadehvandchali,¹²⁶ A. Alkin,³⁴ J. Alme,²¹ T. Alt,⁶⁹ I. Altsybeev,¹¹⁴ M. N. Anaam,⁷ C. Andrei,⁴⁸ D. Andreou,⁹² A. Andronic,¹⁴⁵ M. Angeletti,³⁴ V. Anguelov,¹⁰⁶ F. Antinori,⁵⁷ P. Antonioli,⁵⁴ C. Anuj,¹⁶ N. Apadula,⁸¹ L. Aphecetche,¹¹⁶ H. Appelshäuser,⁶⁹ S. Arcelli,²⁵ R. Arnaldi,⁶⁰ I. C. Arsene,²⁰ M. Arslanok,¹⁴⁷ A. Augustinus,³⁴ R. Averbeck,¹⁰⁹ S. Aziz,⁷⁹ M. D. Azmi,¹⁶ A. Badalà,⁵⁶ Y. W. Baek,⁴¹ X. Bai,^{130,109} R. Bailhache,⁶⁹ Y. Bailung,⁵⁰ R. Bala,¹⁰³ A. Balbino,³⁰ A. Baldisseri,¹³⁹ B. Balis,² D. Banerjee,⁴ R. Barbera,²⁶ L. Barioglio,¹⁰⁷ M. Barlou,⁸⁶ G. G. Barnaföldi,¹⁴⁶ L. S. Barnby,⁹⁶ V. Barret,¹³⁶ C. Bartels,¹²⁹ K. Barth,³⁴ E. Bartsch,⁶⁹ F. Baruffaldi,²⁷ N. Bastid,¹³⁶ S. Basu,⁸² G. Batigne,¹¹⁶ B. Batyunya,⁷⁶ D. Bauri,⁴⁹ J. L. Bazo Alba,¹¹³ I. G. Bearden,⁹¹ C. Beattie,¹⁴⁷ I. Belikov,¹³⁸ A. D. C. Bell Hechavarría,¹⁴⁵ F. Bellini,²⁵ R. Bellwied,¹²⁶ S. Belokurova,¹¹⁴ V. Belyaev,⁹⁵ G. Bencedi,^{146,70} S. Beole,²⁴ A. Bercuci,⁴⁸ Y. Berdnikov,¹⁰⁰ A. Berdnikova,¹⁰⁶ L. Bergmann,¹⁰⁶ M. G. Besoiu,⁶⁸ L. Betev,³⁴ P. P. Bhaduri,¹⁴² A. Bhasin,¹⁰³ I. R. Bhat,¹⁰³ M. A. Bhat,⁴ B. Bhattacharjee,⁴² P. Bhattacharya,²² L. Bianchi,²⁴ N. Bianchi,⁵² J. Bielčák,³⁷ J. Bielčíková,⁹⁷ J. Biernat,¹¹⁹ A. Bilandzic,¹⁰⁷ G. Biro,¹⁴⁶ S. Biswas,⁴ J. T. Blair,¹²⁰ D. Blau,^{90,83} M. B. Blidaru,¹⁰⁹ C. Blume,⁶⁹ G. Boca,^{28,58} F. Bock,⁹⁸ A. Bogdanov,⁹⁵ S. Boi,²² J. Bok,⁶² L. Boldizsár,¹⁴⁶ A. Bolozdynya,⁹⁵ M. Bombara,³⁸ P. M. Bond,³⁴ G. Bonomi,^{141,58} H. Borel,¹³⁹ A. Borissov,⁸³ H. Bossi,¹⁴⁷ E. Botta,²⁴ L. Bratrud,⁶⁹ P. Braun-Munzinger,¹⁰⁹ M. Bregant,¹²² M. Broz,³⁷ G. E. Bruno,^{108,33} M. D. Buckland,¹²⁹ D. Budnikov,¹¹⁰ H. Buesching,⁶⁹ S. Bufalino,³⁰ O. Bugnon,¹¹⁶ P. Buhler,¹¹⁵ Z. Buthelezi,^{73,133} J. B. Butt,¹⁴ A. Bylinkin,¹²⁸ S. A. Bysiak,¹¹⁹ M. Cai,^{27,7} H. Caines,¹⁴⁷ A. Caliva,¹⁰⁹ E. Calvo Villar,¹¹³ J. M. M Camacho,¹²¹ R. S. Camacho,⁴⁵ P. Camerini,²³ F. D. M Canedo,¹²² F. Carnesecchi,^{34,25} R. Caron,¹³⁹ J. Castillo Castellanos,¹³⁹ E. A. R Casula,²² F. Catalano,³⁰ C. Ceballos Sanchez,⁷⁶ P. Chakraborty,⁴⁹ S. Chandra,¹⁴² S. Chapeland,³⁴ M. Chartier,¹²⁹ S. Chattopadhyay,¹⁴² S. Chattopadhyay,¹¹¹ A. Chauvin,²² T. G. Chavez,⁴⁵ T. Cheng,⁷ C. Cheshkov,¹³⁷ B. Cheynis,¹³⁷ V. Chibante Barroso,³⁴ D. D. Chinellato,¹²³ S. Cho,⁶² P. Chochula,³⁴ P. Christakoglou,⁹² C. H. Christensen,⁹¹ P. Christiansen,⁸² T. Chujo,¹³⁵ C. Cicalo,⁵⁵ L. Cifarelli,²⁵ F. Cindolo,⁵⁴ M. R. Ciupek,¹⁰⁹ G. Clai,^{54,a} J. Cleymans,^{125,b} F. Colamaria,⁵³ J. S. Colburn,¹¹² D. Colella,^{53,108,33} A. Collu,⁸¹ M. Colocci,³⁴ M. Concas,^{60,c} G. Conesa Balbastre,⁸⁰ Z. Conesa del Valle,⁷⁹ G. Contin,²³ J. G. Contreras,³⁷ M. L. Coquet,¹³⁹ T. M. Cormier,⁹⁸ P. Cortese,³¹ M. R. Cosentino,¹²⁴ F. Costa,³⁴ S. Costanza,^{28,58} P. Crochet,¹³⁶ R. Cruz-Torres,⁸¹ E. Cuautle,⁷⁰ P. Cui,⁷ L. Cunqueiro,⁹⁸ A. Dainese,⁵⁷ M. C. Danisch,¹⁰⁶ A. Danu,⁶⁸ P. Das,⁸⁸ P. Das,⁴ S. Das,⁴ S. Dash,⁴⁹ A. De Caro,²⁹ G. de Cataldo,⁵³ L. De Cilladi,²⁴ J. de Cuveland,³⁹ A. De Falco,²² D. De Gruttola,²⁹ N. De Marco,⁶⁰ C. De Martin,²³

S. De Pasquale,²⁹ S. Deb,⁵⁰ H. F. Degenhardt,¹²² K. R. Deja,¹⁴³ L. Dello Stritto,²⁹ W. Deng,⁷ P. Dhankher,¹⁹ D. Di Bari,³³ A. Di Mauro,³⁴ R. A. Diaz,⁸ T. Dietel,¹²⁵ Y. Ding,^{137,7} R. Divià,³⁴ D. U. Dixit,¹⁹ Ø. Djuvsland,²¹ U. Dmitrieva,⁶⁴ J. Do,⁶² A. Dobrin,⁶⁸ B. Dönigus,⁶⁹ A. K. Dubey,¹⁴² A. Dubla,^{109,92} S. Dudi,¹⁰² P. Dupieux,¹³⁶ N. Dzalaiova,¹³ T. M. Eder,¹⁴⁵ R. J. Ehlers,⁹⁸ V. N. Eikeland,²¹ F. Eisenhut,⁶⁹ D. Elia,⁵³ B. Erazmus,¹¹⁶ F. Ercolessi,²⁵ F. Erhardt,¹⁰¹ A. Erokhin,¹¹⁴ M. R. Ersdal,²¹ B. Espagnon,⁷⁹ G. Eulisse,³⁴ D. Evans,¹¹² S. Evdokimov,⁹³ L. Fabbietti,¹⁰⁷ M. Faggin,²⁷ J. Faivre,⁸⁰ F. Fan,⁷ A. Fantoni,⁵² M. Fasel,⁹⁸ P. Fecchio,³⁰ A. Feliciello,⁶⁰ G. Feofilov,¹¹⁴ A. Fernández Téllez,⁴⁵ A. Ferrero,¹³⁹ A. Ferretti,²⁴ V. J. G. Feuillard,¹⁰⁶ J. Figiel,¹¹⁹ S. Filchagin,¹¹⁰ D. Finogeev,⁶⁴ F. M. Fionda,^{55,21} G. Fiorenza,^{34,108} F. Flor,¹²⁶ A. N. Flores,¹²⁰ S. Foertsch,⁷³ S. Fokin,⁹⁰ E. Fragiaco,⁶¹ E. Frajna,¹⁴⁶ U. Fuchs,³⁴ N. Funicello,²⁹ C. Furget,⁸⁰ A. Furs,⁶⁴ J. J. Gaardhøje,⁹¹ M. Gagliardi,²⁴ A. M. Gago,¹¹³ A. Gal,¹³⁸ C. D. Galvan,¹²¹ P. Ganoti,⁸⁶ C. Garabatos,¹⁰⁹ J. R. A. Garcia,⁴⁵ E. Garcia-Solis,¹⁰ K. Garg,¹¹⁶ C. Gargiulo,³⁴ A. Garibli,⁸⁹ K. Garner,¹⁴⁵ P. Gasik,¹⁰⁹ E. F. Gauger,¹²⁰ A. Gautam,¹²⁸ M. B. Gay Ducati,⁷¹ M. Germain,¹¹⁶ P. Ghosh,¹⁴² S. K. Ghosh,⁴ M. Giacalone,²⁵ P. Gianotti,⁵² P. Giubellino,^{109,60} P. Giubilato,²⁷ A. M. C. Glaenger,¹³⁹ P. Glässel,¹⁰⁶ D. J. Q. Goh,⁸⁴ V. Gonzalez,¹⁴⁴ L. H. González-Trueba,⁷² S. Gorbunov,³⁹ M. Gorgon,² L. Görlich,¹¹⁹ S. Gotovac,³⁵ V. Grabski,⁷² L. K. Graczykowski,¹⁴³ L. Greiner,⁸¹ A. Grelli,⁶³ C. Grigoras,³⁴ V. Grigoriev,⁹⁵ S. Grigoryan,^{76,1} F. Grosa,^{34,60} J. F. Grosse-Oetringhaus,³⁴ R. Grosso,¹⁰⁹ G. G. Guardiano,¹²³ R. Guernane,⁸⁰ M. Guilbaud,¹¹⁶ K. Gulbrandsen,⁹¹ T. Gunji,¹³⁴ W. Guo,⁷ A. Gupta,¹⁰³ R. Gupta,¹⁰³ S. P. Guzman,⁴⁵ L. Gyulai,¹⁴⁶ M. K. Habib,¹⁰⁹ C. Hadjidakis,⁷⁹ H. Hamagaki,⁸⁴ M. Hamid,⁷ R. Hannigan,¹²⁰ M. R. Haque,¹⁴³ A. Harlanderova,¹⁰⁹ J. W. Harris,¹⁴⁷ A. Harton,¹⁰ J. A. Hasenbichler,³⁴ H. Hassan,⁹⁸ D. Hatzifotiadou,⁵⁴ P. Hauer,⁴³ L. B. Havener,¹⁴⁷ S. T. Heckel,¹⁰⁷ E. Hellbär,¹⁰⁹ H. Helstrup,³⁶ T. Herman,³⁷ E. G. Hernandez,⁴⁵ G. Herrera Corral,⁹ F. Herrmann,¹⁴⁵ K. F. Hetland,³⁶ H. Hillemanns,³⁴ C. Hills,¹²⁹ B. Hippolyte,¹³⁸ B. Hofman,⁶³ B. Hohlweger,⁹² J. Honermann,¹⁴⁵ G. H. Hong,¹⁴⁸ D. Horak,³⁷ S. Hornung,¹⁰⁹ A. Horzyk,² R. Hosokawa,¹⁵ Y. Hou,⁷ P. Hristov,³⁴ C. Hughes,¹³² P. Huhn,⁶⁹ L. M. Huhta,¹²⁷ C. V. Hulse,⁷⁹ T. J. Humanic,⁹⁹ H. Hushnud,¹¹¹ L. A. Husova,¹⁴⁵ A. Hutson,¹²⁶ J. P. Iddon,^{34,129} R. Ilkaev,¹¹⁰ H. Ilyas,¹⁴ M. Inaba,¹³⁵ G. M. Innocenti,³⁴ M. Ippolitov,⁹⁰ A. Isakov,⁷ T. Isidori,¹²⁸ M. S. Islam,¹¹¹ M. Ivanov,¹⁰⁹ V. Ivanov,¹⁰⁰ V. Izucheev,⁹³ M. Jablonski,² B. Jacak,⁸¹ N. Jacazio,³⁴ P. M. Jacobs,⁸¹ S. Jadlovská,¹¹⁸ J. Jadlovsky,¹¹⁸ S. Jaelani,⁶³ C. Jahnke,^{123,122} M. J. Jakubowska,¹⁴³ A. Jalotra,¹⁰³ M. A. Janik,¹⁴³ T. Janson,⁷⁵ M. Jercic,¹⁰¹ O. Jevons,¹¹² A. A. P. Jimenez,⁷⁰ F. Jonas,^{98,145} P. G. Jones,¹¹² J. M. Jowett,^{34,109} J. Jung,⁶⁹ M. Jung,⁶⁹ A. Junjic,³⁴ A. Jusko,¹¹² J. Kaewjai,¹¹⁷ P. Kalinak,⁶⁵ A. S. Kalteyer,¹⁰⁹ A. Kalweit,³⁴ V. Kaplin,⁹⁵ A. Karasu Uysal,⁷⁸ D. Karatovic,¹⁰¹ O. Karavichev,⁶⁴ T. Karavicheva,⁶⁴ P. Karczmarczyk,¹⁴³ E. Karpechev,⁶⁴ V. Kashyap,⁸⁸ A. Kazantsev,⁹⁰ U. Keschull,⁷⁵ R. Keidel,⁴⁷ D. L. D. Keijdener,⁶³ M. Keil,³⁴ B. Ketzer,⁴³ Z. Khabanova,⁹² A. M. Khan,⁷ S. Khan,¹⁶ A. Khanzadeev,¹⁰⁰ Y. Kharlov,^{93,83} A. Khatun,¹⁶ A. Khuntia,¹¹⁹ B. Kileng,³⁶ B. Kim,^{17,62} C. Kim,¹⁷ D. J. Kim,¹²⁷ E. J. Kim,⁷⁴ J. Kim,¹⁴⁸ J. S. Kim,⁴¹ J. Kim,¹⁰⁶ J. Kim,⁷⁴ M. Kim,¹⁰⁶ S. Kim,¹⁸ T. Kim,¹⁴⁸ S. Kirsch,⁶⁹ I. Kisel,³⁹ S. Kiselev,⁹⁴ A. Kisiel,¹⁴³ J. P. Kitowski,² J. L. Klay,⁶ J. Klein,³⁴ S. Klein,⁸¹ C. Klein-Bösing,¹⁴⁵ M. Kleiner,⁶⁹ T. Klemenz,¹⁰⁷ A. Kluge,³⁴ A. G. Knospe,¹²⁶ C. Kobdaj,¹¹⁷ M. K. Köhler,¹⁰⁶ T. Kollegger,¹⁰⁹ A. Kondratyev,⁷⁶ N. Kondratyeva,⁹⁵ E. Kondratyuk,⁹³ J. König,⁶⁹ S. A. Königstorfer,¹⁰⁷ P. J. Konopka,³⁴ G. Kornakov,¹⁴³ S. D. Koryciak,² A. Kotliarov,⁹⁷ O. Kovalenko,⁸⁷ V. Kovalenko,¹¹⁴ M. Kowalski,¹¹⁹ I. Králik,⁶⁵ A. Kravčáková,³⁸ L. Kreis,¹⁰⁹ M. Krivda,^{112,65} F. Krizek,⁹⁷ K. Krizkova Gajdosova,³⁷ M. Kroesen,¹⁰⁶ M. Krüger,⁶⁹ E. Kryshen,¹⁰⁰ M. Krzewicki,³⁹ V. Kučera,³⁴ C. Kuhn,¹³⁸ P. G. Kuijper,⁹² T. Kumaoka,¹³⁵ D. Kumar,¹⁴² L. Kumar,¹⁰² N. Kumar,¹⁰² S. Kundu,³⁴ P. Kurashvili,⁸⁷ A. Kurepin,⁶⁴ A. B. Kurepin,⁶⁴ A. Kuryakin,¹¹⁰ S. Kuschpil,⁹⁷ J. Kvapil,¹¹² M. J. Kweon,⁶² J. Y. Kwon,⁶² Y. Kwon,¹⁴⁸ S. L. La Pointe,³⁹ P. La Rocca,²⁶ Y. S. Lai,⁸¹ A. Lakrathok,¹¹⁷ M. Lamanna,³⁴ R. Langoy,¹³¹ K. Lapidus,³⁴ P. Larionov,^{34,52} E. Laudi,³⁴ L. Lautner,^{34,107} R. Lavicka,^{115,37} T. Lazareva,¹¹⁴ R. Lea,^{141,23,58} J. Leibrach,³⁹ R. C. Lemmon,⁹⁶ I. León Monzón,¹²¹ E. D. Lesser,¹⁹ M. Lettrich,^{34,107} P. Lévai,¹⁴⁶ X. Li,¹¹ X. L. Li,⁷ J. Lien,¹³¹ R. Lietava,¹¹² B. Lim,¹⁷ S. H. Lim,¹⁷ V. Lindenstruth,³⁹ A. Lindner,⁴⁸ C. Lippmann,¹⁰⁹ A. Liu,¹⁹ D. H. Liu,⁷ J. Liu,¹²⁹ I. M. Lofnes,²¹ V. Loginov,⁹⁵ C. Loizides,⁹⁸ P. Loncar,³⁵ J. A. Lopez,¹⁰⁶ X. Lopez,¹³⁶ E. López Torres,⁸ J. R. Luhder,¹⁴⁵ M. Lunardon,²⁷ G. Luparello,⁶¹ Y. G. Ma,⁴⁰ A. Maevskaya,⁶⁴ M. Mager,³⁴ T. Mahmoud,⁴³ A. Maire,¹³⁸ M. Malaev,¹⁰⁰ N. M. Malik,¹⁰³ Q. W. Malik,²⁰ S. K. Malik,¹⁰³ L. Malinina,^{76,d} D. Mal'Kevich,⁹⁴ D. Mallick,⁸⁸ N. Mallick,⁵⁰ G. Mandaglio,^{32,56} V. Manko,⁹⁰ F. Manso,¹³⁶ V. Manzari,⁵³ Y. Mao,⁷ G. V. Margagliotti,²³ A. Margotti,⁵⁴ A. Marín,¹⁰⁹ C. Markert,¹²⁰ M. Marquard,⁶⁹ N. A. Martin,⁵⁵ P. Martinengo,³⁴ J. L. Martinez,¹²⁶ M. I. Martínez,⁴⁵ G. Martínez García,¹¹⁶ S. Masciocchi,¹⁰⁹ M. Masera,²⁴ A. Masoni,⁵⁵ L. Massacrier,⁷⁹ A. Mastroserio,^{140,53} A. M. Mathis,¹⁰⁷ O. Matonoha,⁸² P. F. T. Matuoka,¹²² A. Matyja,¹¹⁹ C. Mayer,¹¹⁹ A. L. Mazuecos,³⁴ F. Mazzaschi,²⁴ M. Mazzilli,³⁴ M. A. Mazzoni,^{59,b} J. E. Mdhuli,¹³³ A. F. Mechler,⁶⁹ Y. Melikyan,⁶⁴ A. Menchaca-Rocha,⁷² E. Meninno,^{115,29} A. S. Menon,¹²⁶ M. Meres,¹³ S. Mhlanga,^{125,73} Y. Miake,¹³⁵ L. Micheletti,⁶⁰ L. C. Migliorin,¹³⁷ D. L. Mihaylov,¹⁰⁷ K. Mikhaylov,^{76,94} A. N. Mishra,¹⁴⁶ D. Miśkowiec,¹⁰⁹ A. Modak,⁴ A. P. Mohanty,⁶³ B. Mohanty,⁸⁸ M. Mohisin Khan,^{16,e} M. A. Molander,⁴⁴ Z. Moravcova,⁹¹ C. Mordasini,¹⁰⁷ D. A. Moreira De Godoy,¹⁴⁵ I. Morozov,⁶⁴ A. Morsch,³⁴ T. Mrnjavac,³⁴ V. Muccifora,⁵² E. Mudnic,³⁵ D. Mühlheim,¹⁴⁵ S. Muhuri,¹⁴² J. D. Mulligan,⁸¹ A. Mulliri,²² M. G. Munhoz,¹²² R. H. Munzer,⁶⁹ H. Murakami,¹³⁴ S. Murray,¹²⁵ L. Musa,³⁴ J. Musinsky,⁶⁵ J. W. Myrcha,¹⁴³ B. Naik,^{133,49} R. Nair,⁸⁷ B. K. Nandi,⁴⁹ R. Nania,⁵⁴ E. Nappi,⁵³ A. F. Nassirpour,⁸² A. Nath,¹⁰⁶ C. Natrass,¹³² A. Neagu,²⁰ L. Nellen,⁷⁰ S. V. Nesbo,³⁶ G. Neskovic,³⁹ D. Nesterov,¹¹⁴ B. S. Nielsen,⁹¹ S. Nikolaev,⁹⁰ S. Nikulin,⁹⁰ V. Nikulin,¹⁰⁰ F. Noferini,⁵⁴ S. Noh,¹² P. Nomokonov,⁷⁶ J. Norman,¹²⁹ N. Novitzky,¹³⁵ P. Nowakowski,¹⁴³ A. Nyanin,⁹⁰ J. Nystrand,²¹ M. Ogino,⁸⁴ A. Ohlson,⁸² V. A. Okorokov,⁹⁵ J. Oleniacz,¹⁴³ A. C. Oliveira Da Silva,¹³² M. H. Oliver,¹⁴⁷ A. Onnerstad,¹²⁷ C. Oppedisano,⁶⁰ A. Ortiz Velasquez,⁷⁰ T. Osako,⁴⁶ A. Oskarsson,⁸² J. Otwinowski,¹¹⁹ M. Oya,⁴⁶ K. Oyama,⁸⁴ Y. Pachmayer,¹⁰⁶ S. Padhan,⁴⁹ D. Pagano,^{141,58} G. Pačić,⁷⁰ A. Palasciano,⁵³ J. Pan,¹⁴⁴ S. Panebianco,¹³⁹ J. Park,⁶² J. E. Parkkila,¹²⁷ S. P. Pathak,¹²⁶

R. N. Patra,^{103,34} B. Paul,²² H. Pei,⁷ T. Peitzmann,⁶³ X. Peng,⁷ L. G. Pereira,⁷¹ H. Pereira Da Costa,¹³⁹ D. Peresunko,^{90,83} G. M. Perez,⁸ S. Perrin,¹³⁹ Y. Pestov,⁵ V. Petráček,³⁷ M. Petrovici,⁴⁸ R. P. Pezzi,^{116,71} S. Piano,⁶¹ M. Pikna,¹³ P. Pillot,¹¹⁶ O. Pinazza,^{54,34} L. Pinsky,¹²⁶ C. Pinto,²⁶ S. Pisano,⁵² M. Płoskoń,⁸¹ M. Planinic,¹⁰¹ F. Pliquett,⁶⁹ M. G. Poghosyan,⁹⁸ B. Polichtchouk,⁹³ S. Politano,³⁰ N. Poljak,¹⁰¹ A. Pop,⁴⁸ S. Porteboeuf-Houssais,¹³⁶ J. Porter,⁸¹ V. Pozdniakov,⁷⁶ S. K. Prasad,⁴ R. Preghenella,⁵⁴ F. Prino,⁶⁰ C. A. Pruneau,¹⁴⁴ I. Pshenichnov,⁶⁴ M. Puccio,³⁴ S. Qiu,⁹² L. Quaglia,²⁴ R. E. Quishpe,¹²⁶ S. Ragoni,¹¹² A. Rakotozafindrabe,¹³⁹ L. Ramello,³¹ F. Rami,¹³⁸ S. A. R. Ramirez,⁴⁵ A. G. T. Ramos,³³ T. A. Rancien,⁸⁰ R. Raniwala,¹⁰⁴ S. Raniwala,¹⁰⁴ S. S. Räsänen,⁴⁴ R. Rath,⁵⁰ I. Ravasenga,⁹² K. F. Read,^{98,132} A. R. Redelbach,³⁹ K. Redlich,^{87,f} A. Rehman,²¹ P. Reichelt,⁶⁹ F. Reidt,³⁴ H. A. Reme-ness,³⁶ Z. Rescakova,³⁸ K. Reygers,¹⁰⁶ A. Riabov,¹⁰⁰ V. Riabov,¹⁰⁰ T. Richert,⁸² M. Richter,²⁰ W. Riegler,³⁴ F. Riggi,²⁶ C. Ristea,⁶⁸ M. Rodríguez Cahuantzi,⁴⁵ K. Røed,²⁰ R. Rogalev,⁹³ E. Rogochaya,⁷⁶ T. S. Rogoschinski,⁶⁹ D. Rohr,³⁴ D. Röhrich,²¹ P. F. Rojas,⁴⁵ P. S. Rokita,¹⁴³ F. Ronchetti,⁵² A. Rosano,^{32,56} E. D. Rosas,⁷⁰ A. Rossi,⁵⁷ A. Roy,⁵⁰ P. Roy,¹¹¹ S. Roy,⁴⁹ N. Rubini,²⁵ O. V. Rueda,⁸² D. Ruggiano,¹⁴³ R. Rui,²³ B. Rumyantsev,⁷⁶ P. G. Russek,² R. Russo,⁹² A. Rustamov,⁸⁹ E. Ryabinkin,⁹⁰ Y. Ryabov,¹⁰⁰ A. Rybicki,¹¹⁹ H. Rytkonen,¹²⁷ W. Rzesza,¹⁴³ O. A. M. Saarimäki,⁴⁴ R. Sadek,¹¹⁶ S. Sadovsky,⁹³ J. Saetre,²¹ K. Šafařík,³⁷ S. K. Saha,¹⁴² S. Saha,⁸⁸ B. Sahoo,⁴⁹ P. Sahoo,⁴⁹ R. Sahoo,⁵⁰ S. Sahoo,⁶⁶ D. Sahu,⁵⁰ P. K. Sahu,⁶⁶ J. Saini,¹⁴² S. Sakai,¹³⁵ M. P. Salvan,¹⁰⁹ S. Sambyal,¹⁰³ V. Samsonov,^{100,95,b} D. Sarkar,¹⁴⁴ N. Sarkar,¹⁴² P. Sarma,⁴² V. M. Sarti,¹⁰⁷ M. H. P. Sas,¹⁴⁷ J. Schambach,⁹⁸ H. S. Scheid,⁶⁹ C. Schiaua,⁴⁸ R. Schicker,¹⁰⁶ A. Schmah,¹⁰⁶ C. Schmidt,¹⁰⁹ H. R. Schmidt,¹⁰⁵ M. O. Schmidt,^{34,106} M. Schmidt,¹⁰⁵ N. V. Schmidt,^{98,69} A. R. Schmier,¹³² R. Schotter,¹³⁸ J. Schukraft,³⁴ K. Schwarz,¹⁰⁹ K. Schweda,¹⁰⁹ G. Scioli,²⁵ E. Scomparin,⁶⁰ J. E. Seger,¹⁵ Y. Sekiguchi,¹³⁴ D. Sekihata,¹³⁴ I. Selyuzhenkov,^{109,95} S. Senyukov,¹³⁸ J. J. Seo,⁶² D. Serebryakov,⁶⁴ L. Šeršňnyte,¹⁰⁷ A. Sevcenco,⁶⁸ T. J. Shaba,⁷³ A. Shabanov,⁶⁴ A. Shabetai,¹¹⁶ R. Shahoyan,³⁴ W. Shaikh,¹¹¹ A. Shangaraev,⁹³ A. Sharma,¹⁰² H. Sharma,¹¹⁹ M. Sharma,¹⁰³ N. Sharma,¹⁰² S. Sharma,¹⁰³ U. Sharma,¹⁰³ O. Sheibani,¹²⁶ K. Shigaki,⁴⁶ M. Shimomura,⁸⁵ S. Shirinkin,⁹⁴ Q. Shou,⁴⁰ Y. Sibiriyak,⁹⁰ S. Siddhanta,⁵⁵ T. Siemiarczuk,⁸⁷ T. F. Silva,¹²² D. Silvermyr,⁸² T. Simantathammakul,¹¹⁷ G. Simonetti,³⁴ B. Singh,¹⁰⁷ R. Singh,⁸⁸ R. Singh,¹⁰³ R. Singh,⁵⁰ V. K. Singh,¹⁴² V. Singhal,¹⁴² T. Sinha,¹¹¹ B. Sitar,¹³ M. Sitta,³¹ T. B. Skaali,²⁰ G. Skorodumovs,¹⁰⁶ M. Slupecki,⁴⁴ N. Smirnov,¹⁴⁷ R. J. M. Snellings,⁶³ C. Soncco,¹¹³ J. Song,¹²⁶ A. Songmoolnak,¹¹⁷ F. Soramel,²⁷ S. Sorensen,¹³² I. Sputowska,¹¹⁹ J. Stachel,¹⁰⁶ I. Stan,⁶⁸ P. J. Steffanic,¹³² S. F. Stiefelmaier,¹⁰⁶ D. Stocco,¹¹⁶ I. Storehaug,²⁰ M. M. Storetvedt,³⁶ P. Stratmann,¹⁴⁵ C. P. Stylianidis,⁹² A. A. P. Suaide,¹²² C. Suire,⁷⁹ M. Sukhanov,⁶⁴ M. Suljic,³⁴ R. Sultanov,⁹⁴ V. Summeria,¹⁰³ S. Sumowidagdo,⁵¹ S. Swain,⁶⁶ A. Szabo,¹³ I. Szarka,¹³ U. Tabassam,¹⁴ S. F. Taghavi,¹⁰⁷ G. Tallepied,¹³⁶ J. Takahashi,¹²³ G. J. Tambave,²¹ S. Tang,^{136,7} Z. Tang,¹³⁰ J. D. Tapia Takaki,^{128,g} M. Tarhini,¹¹⁶ M. G. Tarzila,⁴⁸ A. Tauro,³⁴ G. Tejada Muñoz,⁴⁵ A. Telesca,³⁴ L. Terlizzi,²⁴ C. Terrevoli,¹²⁶ G. Tersimonov,³ S. Thakur,¹⁴² D. Thomas,¹²⁰ R. Tieulent,¹³⁷ A. Tikhonov,⁶⁴ A. R. Timmins,¹²⁶ M. Tkacik,¹¹⁸ A. Toia,⁶⁹ N. Topilskaya,⁶⁴ M. Toppi,⁵² F. Torres-Acosta,¹⁹ T. Tork,⁷⁹ S. R. Torres,³⁷ A. Trifiró,^{32,56} S. Tripathy,^{54,70} T. Tripathy,⁴⁹ S. Trogolo,^{34,27} V. Trubnikov,³ W. H. Trzaska,¹²⁷ T. P. Trzcinski,¹⁴³ A. Tumkin,¹¹⁰ R. Turrisi,⁵⁷ T. S. Tveter,²⁰ K. Ullaland,²¹ A. Uras,¹³⁷ M. Urioni,^{58,141} G. L. Usai,²² M. Vala,³⁸ N. Valle,^{28,58} S. Vallero,⁶⁰ L. V. R. van Doremalen,⁶³ M. van Leeuwen,⁹² R. J. G. van Weelden,⁹² P. Vande Vyvre,³⁴ D. Varga,¹⁴⁶ Z. Varga,¹⁴⁶ M. Varga-Kofarago,¹⁴⁶ M. Vasileiou,⁸⁶ A. Vasiliev,⁹⁰ O. Vázquez Doce,^{52,107} V. Vechernin,¹¹⁴ E. Vercellin,²⁴ S. Vergara Limón,⁴⁵ L. Vermunt,⁶³ R. Vértesi,¹⁴⁶ M. Verweij,⁶³ L. Vickovic,³⁵ Z. Vilakazi,¹³³ O. Villalobos Baillie,¹¹² G. Vino,⁵³ A. Vinogradov,⁹⁰ T. Virgili,²⁹ V. Vislavicius,⁹¹ A. Vodopyanov,⁷⁶ B. Volkel,^{34,106} M. A. Völkl,¹⁰⁶ K. Voloshin,⁹⁴ S. A. Voloshin,¹⁴⁴ G. Volpe,³³ B. von Haller,³⁴ I. Vorobyev,¹⁰⁷ D. Voscek,¹¹⁸ N. Vozniuk,⁶⁴ J. Vrláková,³⁸ B. Wagner,²¹ C. Wang,⁴⁰ D. Wang,⁴⁰ M. Weber,¹¹⁵ A. Wegrzynek,³⁴ S. C. Wenzel,³⁴ J. P. Wessels,¹⁴⁵ J. Wiechula,⁶⁹ J. Wikne,²⁰ G. Wilk,⁸⁷ J. Wilkinson,¹⁰⁹ G. A. Willems,¹⁴⁵ B. Windelband,¹⁰⁶ M. Winn,¹³⁹ W. E. Witt,¹³² J. R. Wright,¹²⁰ W. Wu,⁴⁰ Y. Wu,¹³⁰ R. Xu,⁷ A. K. Yadav,¹⁴² S. Yalcin,⁷⁸ Y. Yamaguchi,⁴⁶ K. Yamakawa,⁴⁶ S. Yang,²¹ S. Yano,⁴⁶ Z. Yin,⁷ I.-K. Yoo,¹⁷ J. H. Yoon,⁶² S. Yuan,²¹ A. Yuncu,¹⁰⁶ V. Zaccolo,²³ C. Zampolli,³⁴ H. J. C. Zanoli,⁶³ N. Zardoshti,³⁴ A. Zarochentsev,¹¹⁴ P. Závada,⁶⁷ N. Zaviyalov,¹¹⁰ M. Zhalov,¹⁰⁰ B. Zhang,⁷ S. Zhang,⁴⁰ X. Zhang,⁷ Y. Zhang,¹³⁰ V. Zhrebchevskii,¹¹⁴ Y. Zhi,¹¹ N. Zhigareva,⁹⁴ D. Zhou,⁷ Y. Zhou,⁹¹ J. Zhu,^{109,7} Y. Zhu,⁷ G. Zinovjev,³ and N. Zurlo^{141,58}

(ALICE Collaboration)

¹A.I. Alikhanyan National Science Laboratory (Yerevan Physics Institute) Foundation, Yerevan, Armenia²AGH University of Science and Technology, Cracow, Poland³Bogolyubov Institute for Theoretical Physics, National Academy of Sciences of Ukraine, Kiev, Ukraine⁴Bose Institute, Department of Physics and Centre for Astroparticle Physics and Space Science (CAPSS), Kolkata, India⁵Budker Institute for Nuclear Physics, Novosibirsk, Russia⁶California Polytechnic State University, San Luis Obispo, California, USA⁷Central China Normal University, Wuhan, China⁸Centro de Aplicaciones Tecnológicas y Desarrollo Nuclear (CEADEN), Havana, Cuba⁹Centro de Investigación y de Estudios Avanzados (CINVESTAV), Mexico City and Mérida, Mexico¹⁰Chicago State University, Chicago, Illinois, USA¹¹China Institute of Atomic Energy, Beijing, China¹²Chungbuk National University, Cheongju, Republic of Korea

- ¹³Comenius University Bratislava, Faculty of Mathematics, Physics and Informatics, Bratislava, Slovakia
- ¹⁴COMSATS University Islamabad, Islamabad, Pakistan
- ¹⁵Creighton University, Omaha, Nebraska, USA
- ¹⁶Department of Physics, Aligarh Muslim University, Aligarh, India
- ¹⁷Department of Physics, Pusan National University, Pusan, Republic of Korea
- ¹⁸Department of Physics, Sejong University, Seoul, Republic of Korea
- ¹⁹Department of Physics, University of California, Berkeley, California, USA
- ²⁰Department of Physics, University of Oslo, Oslo, Norway
- ²¹Department of Physics and Technology, University of Bergen, Bergen, Norway
- ²²Dipartimento di Fisica dell'Università and Sezione INFN, Cagliari, Italy
- ²³Dipartimento di Fisica dell'Università and Sezione INFN, Trieste, Italy
- ²⁴Dipartimento di Fisica dell'Università and Sezione INFN, Turin, Italy
- ²⁵Dipartimento di Fisica e Astronomia dell'Università and Sezione INFN, Bologna, Italy
- ²⁶Dipartimento di Fisica e Astronomia dell'Università and Sezione INFN, Catania, Italy
- ²⁷Dipartimento di Fisica e Astronomia dell'Università and Sezione INFN, Padova, Italy
- ²⁸Dipartimento di Fisica e Nucleare e Teorica, Università di Pavia, Pavia, Italy
- ²⁹Dipartimento di Fisica 'E.R. Caianiello' dell'Università and Gruppo Collegato INFN, Salerno, Italy
- ³⁰Dipartimento DISAT del Politecnico and Sezione INFN, Turin, Italy
- ³¹Dipartimento di Scienze e Innovazione Tecnologica dell'Università del Piemonte Orientale and INFN Sezione di Torino, Alessandria, Italy
- ³²Dipartimento di Scienze MIFT, Università di Messina, Messina, Italy
- ³³Dipartimento Interateneo di Fisica 'M. Merlin' and Sezione INFN, Bari, Italy
- ³⁴European Organization for Nuclear Research (CERN), Geneva, Switzerland
- ³⁵Faculty of Electrical Engineering, Mechanical Engineering and Naval Architecture, University of Split, Split, Croatia
- ³⁶Faculty of Engineering and Science, Western Norway University of Applied Sciences, Bergen, Norway
- ³⁷Faculty of Nuclear Sciences and Physical Engineering, Czech Technical University in Prague, Prague, Czech Republic
- ³⁸Faculty of Science, P.J. Šafárik University, Košice, Slovakia
- ³⁹Frankfurt Institute for Advanced Studies, Johann Wolfgang Goethe-Universität Frankfurt, Frankfurt, Germany
- ⁴⁰Fudan University, Shanghai, China
- ⁴¹Gangneung-Wonju National University, Gangneung, Republic of Korea
- ⁴²Gauhati University, Department of Physics, Guwahati, India
- ⁴³Helmholtz-Institut für Strahlen- und Kernphysik, Rheinische Friedrich-Wilhelms-Universität Bonn, Bonn, Germany
- ⁴⁴Helsinki Institute of Physics (HIP), Helsinki, Finland
- ⁴⁵High Energy Physics Group, Universidad Autónoma de Puebla, Puebla, Mexico
- ⁴⁶Hiroshima University, Hiroshima, Japan
- ⁴⁷Hochschule Worms, Zentrum für Technologietransfer und Telekommunikation (ZTT), Worms, Germany
- ⁴⁸Horia Hulubei National Institute of Physics and Nuclear Engineering, Bucharest, Romania
- ⁴⁹Indian Institute of Technology Bombay (IIT), Mumbai, India
- ⁵⁰Indian Institute of Technology Indore, Indore, India
- ⁵¹Indonesian Institute of Sciences, Jakarta, Indonesia
- ⁵²INFN, Laboratori Nazionali di Frascati, Frascati, Italy
- ⁵³INFN, Sezione di Bari, Bari, Italy
- ⁵⁴INFN, Sezione di Bologna, Bologna, Italy
- ⁵⁵INFN, Sezione di Cagliari, Cagliari, Italy
- ⁵⁶INFN, Sezione di Catania, Catania, Italy
- ⁵⁷INFN, Sezione di Padova, Padova, Italy
- ⁵⁸INFN, Sezione di Pavia, Pavia, Italy
- ⁵⁹INFN, Sezione di Roma, Rome, Italy
- ⁶⁰INFN, Sezione di Torino, Turin, Italy
- ⁶¹INFN, Sezione di Trieste, Trieste, Italy
- ⁶²Inha University, Incheon, Republic of Korea
- ⁶³Institute for Gravitational and Subatomic Physics (GRASP), Utrecht University/Nikhef, Utrecht, Netherlands
- ⁶⁴Institute for Nuclear Research, Academy of Sciences, Moscow, Russia
- ⁶⁵Institute of Experimental Physics, Slovak Academy of Sciences, Košice, Slovakia
- ⁶⁶Institute of Physics, Homi Bhabha National Institute, Bhubaneswar, India
- ⁶⁷Institute of Physics of the Czech Academy of Sciences, Prague, Czech Republic
- ⁶⁸Institute of Space Science (ISS), Bucharest, Romania
- ⁶⁹Institut für Kernphysik, Johann Wolfgang Goethe-Universität Frankfurt, Frankfurt, Germany
- ⁷⁰Instituto de Ciencias Nucleares, Universidad Nacional Autónoma de México, Mexico City, Mexico
- ⁷¹Instituto de Física, Universidade Federal do Rio Grande do Sul (UFRGS), Porto Alegre, Brazil

- ⁷²*Instituto de Física, Universidad Nacional Autónoma de México, Mexico City, Mexico*
- ⁷³*iThemba LABS, National Research Foundation, Somerset West, South Africa*
- ⁷⁴*Jeonbuk National University, Jeonju, Republic of Korea*
- ⁷⁵*Johann-Wolfgang-Goethe Universität Frankfurt Institut für Informatik, Fachbereich Informatik und Mathematik, Frankfurt, Germany*
- ⁷⁶*Joint Institute for Nuclear Research (JINR), Dubna, Russia*
- ⁷⁷*Korea Institute of Science and Technology Information, Daejeon, Republic of Korea*
- ⁷⁸*KTO Karatay University, Konya, Turkey*
- ⁷⁹*Laboratoire de Physique des 2 Infinis, Irène Joliot-Curie, Orsay, France*
- ⁸⁰*Laboratoire de Physique Subatomique et de Cosmologie, Université Grenoble-Alpes, CNRS-IN2P3, Grenoble, France*
- ⁸¹*Lawrence Berkeley National Laboratory, Berkeley, California, USA*
- ⁸²*Lund University Department of Physics, Division of Particle Physics, Lund, Sweden*
- ⁸³*Moscow Institute for Physics and Technology, Moscow, Russia*
- ⁸⁴*Nagasaki Institute of Applied Science, Nagasaki, Japan*
- ⁸⁵*Nara Women's University (NWU), Nara, Japan*
- ⁸⁶*National and Kapodistrian University of Athens, School of Science, Department of Physics, Athens, Greece*
- ⁸⁷*National Centre for Nuclear Research, Warsaw, Poland*
- ⁸⁸*National Institute of Science Education and Research, Homi Bhabha National Institute, Jatni, India*
- ⁸⁹*National Nuclear Research Center, Baku, Azerbaijan*
- ⁹⁰*National Research Centre Kurchatov Institute, Moscow, Russia*
- ⁹¹*Niels Bohr Institute, University of Copenhagen, Copenhagen, Denmark*
- ⁹²*Nikhef, National institute for subatomic physics, Amsterdam, Netherlands*
- ⁹³*NRC Kurchatov Institute IHEP, Protvino, Russia*
- ⁹⁴*NRC «Kurchatov» Institute - ITEP, Moscow, Russia*
- ⁹⁵*NRNU Moscow Engineering Physics Institute, Moscow, Russia*
- ⁹⁶*Nuclear Physics Group, STFC Daresbury Laboratory, Daresbury, United Kingdom*
- ⁹⁷*Nuclear Physics Institute of the Czech Academy of Sciences, Řež u Prahy, Czech Republic*
- ⁹⁸*Oak Ridge National Laboratory, Oak Ridge, Tennessee, USA*
- ⁹⁹*Ohio State University, Columbus, Ohio, USA*
- ¹⁰⁰*Petersburg Nuclear Physics Institute, Gatchina, Russia*
- ¹⁰¹*Physics department, Faculty of science, University of Zagreb, Zagreb, Croatia*
- ¹⁰²*Physics Department, Panjab University, Chandigarh, India*
- ¹⁰³*Physics Department, University of Jammu, Jammu, India*
- ¹⁰⁴*Physics Department, University of Rajasthan, Jaipur, India*
- ¹⁰⁵*Physikalisches Institut, Eberhard-Karls-Universität Tübingen, Tübingen, Germany*
- ¹⁰⁶*Physikalisches Institut, Ruprecht-Karls-Universität Heidelberg, Heidelberg, Germany*
- ¹⁰⁷*Physik Department, Technische Universität München, Munich, Germany*
- ¹⁰⁸*Politecnico di Bari and Sezione INFN, Bari, Italy*
- ¹⁰⁹*Research Division and ExtreMe Matter Institute EMMI, GSI Helmholtzzentrum für Schwerionenforschung GmbH, Darmstadt, Germany*
- ¹¹⁰*Russian Federal Nuclear Center (VNIIEF), Sarov, Russia*
- ¹¹¹*Saha Institute of Nuclear Physics, Homi Bhabha National Institute, Kolkata, India*
- ¹¹²*School of Physics and Astronomy, University of Birmingham, Birmingham, United Kingdom*
- ¹¹³*Sección Física, Departamento de Ciencias, Pontificia Universidad Católica del Perú, Lima, Peru*
- ¹¹⁴*St. Petersburg State University, St. Petersburg, Russia*
- ¹¹⁵*Stefan Meyer Institut für Subatomare Physik (SMI), Vienna, Austria*
- ¹¹⁶*SUBATECH, IMT Atlantique, Université de Nantes, CNRS-IN2P3, Nantes, France*
- ¹¹⁷*Suranaree University of Technology, Nakhon Ratchasima, Thailand*
- ¹¹⁸*Technical University of Košice, Košice, Slovakia*
- ¹¹⁹*The Henryk Niewodniczanski Institute of Nuclear Physics, Polish Academy of Sciences, Cracow, Poland*
- ¹²⁰*The University of Texas at Austin, Austin, Texas, USA*
- ¹²¹*Universidad Autónoma de Sinaloa, Culiacán, Mexico*
- ¹²²*Universidade de São Paulo (USP), São Paulo, Brazil*
- ¹²³*Universidade Estadual de Campinas (UNICAMP), Campinas, Brazil*
- ¹²⁴*Universidade Federal do ABC, Santo Andre, Brazil*
- ¹²⁵*University of Cape Town, Cape Town, South Africa*
- ¹²⁶*University of Houston, Houston, Texas, USA*
- ¹²⁷*University of Jyväskylä, Jyväskylä, Finland*
- ¹²⁸*University of Kansas, Lawrence, Kansas, USA*
- ¹²⁹*University of Liverpool, Liverpool, United Kingdom*
- ¹³⁰*University of Science and Technology of China, Hefei, China*

¹³¹*University of South-Eastern Norway, Tonsberg, Norway*

¹³²*University of Tennessee, Knoxville, Tennessee, USA*

¹³³*University of the Witwatersrand, Johannesburg, South Africa*

¹³⁴*University of Tokyo, Tokyo, Japan*

¹³⁵*University of Tsukuba, Tsukuba, Japan*

¹³⁶*Université Clermont Auvergne, CNRS/IN2P3, LPC, Clermont-Ferrand, France*

¹³⁷*Université de Lyon, CNRS/IN2P3, Institut de Physique des 2 Infinis de Lyon, Lyon, France*

¹³⁸*Université de Strasbourg, CNRS, IPHC UMR 7178, F-67000 Strasbourg, France, Strasbourg, France*

¹³⁹*Université Paris-Saclay Centre d'Etudes de Saclay (CEA), IRFU, Département de Physique Nucléaire (DPhN), Saclay, France*

¹⁴⁰*Università degli Studi di Foggia, Foggia, Italy*

¹⁴¹*Università di Brescia, Brescia, Italy*

¹⁴²*Variable Energy Cyclotron Centre, Homi Bhabha National Institute, Kolkata, India*

¹⁴³*Warsaw University of Technology, Warsaw, Poland*

¹⁴⁴*Wayne State University, Detroit, Michigan, USA*

¹⁴⁵*Westfälische Wilhelms-Universität Münster, Institut für Kernphysik, Münster, Germany*

¹⁴⁶*Wigner Research Centre for Physics, Budapest, Hungary*

¹⁴⁷*Yale University, New Haven, Connecticut, USA*

¹⁴⁸*Yonsei University, Seoul, Republic of Korea*

^aAlso at: Italian National Agency for New Technologies, Energy and Sustainable Economic Development (ENEA), Bologna, Italy.

^bDeceased.

^cAlso at: Dipartimento DET del Politecnico di Torino, Turin, Italy.

^dAlso at: M.V. Lomonosov Moscow State University, D.V. Skobeltsyn Institute of Nuclear Physics, Moscow, Russia.

^eAlso at: Department of Applied Physics, Aligarh Muslim University, Aligarh, India.

^fAlso at: Institute of Theoretical Physics, University of Wrocław, Poland.

^gAlso at: University of Kansas, Lawrence, Kansas, USA.